ORGANOMETALLICS

pubs.acs.org/Organometallics Article

Oxidation of Methylplatinum(II) Complexes K[(L)Pt^{II}Me] with O_2 and C(sp^3)-X (X = O and C) Reductive Elimination Reactivity of Methylplatinum(IV) Products (*L*)Pt^{IV}Me(OH): The Effect of Structure of Sulfonated CNN-Pincer Ligands L

Jiaheng Ruan, Daoyong Wang, Morgan J. Kramer, Peter Y. Zavalij, and Andrei N. Vedernikov*

Cite This: *Organometallics* 2022, 41, 2764–2783 Read Online

ACCESS | Metrics & More | Article Recommendations | Supporting Information

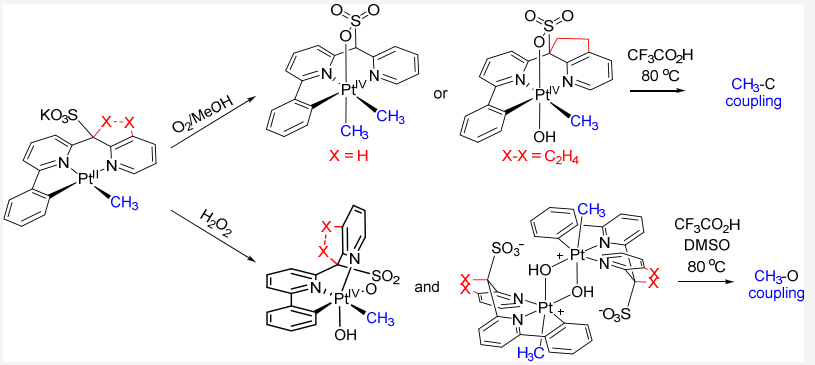

ABSTRACT: Two sulfonated CNN-pincer ligands L1 and L2 were used to explore the oxidative functionalization of the Pt^{II}-Me bond in derived K[(L)Pt^{II}Me] complexes (L = L1 and L2) using O_2 and H_2O_2 as oxidants ($HL1^-$ = (6-phenylpyrid-2-yl)(pyrid-2-yl)methanesulfonate; $HL2^-$ = (6-phenylpyrid-2-yl)-6,7-dihydro-5H-cyclopenta [*b*]pyridine-7-sulfonate). Oxidation with O_2 of K[(L1)Pt^{II}Me] in MeOH produced a single high-valent platinum complex, (L1)Pt^{IV}Me$_2$, whereas the use of H_2O_2 led to (L1)Pt^{IV}Me(OH), **10c**, and (L1)$_2$Pt$^{IV}_2$Me$_2$(μ-OH)$_2$, **14**, having different configurations of a Pt^{IV} center. Oxidation of a more rigid analog, K[(L2)Pt^{II}Me], with O_2 led to diastereomeric complexes (L2)Pt^{IV}Me(OH), **11d**, in MeOH and **11a** (detected as an adduct with the $CF_3CH_2O^-$ anion) in acetone/2,2,2-trifluoroethanol mixtures. The use of H_2O_2 led to (L2)Pt^{IV}Me(OH), **11c**, and (L2)$_2$Pt$^{IV}_2$Me$_2$(μ-OH)$_2$, **15**, the analogs of **10c** and **14**, respectively. When heated with CF_3CO_2H in aqueous DMSO, MeOH, or acetone at 80 °C, (L)Pt^{IV}Me(OH) complexes produced in high yield either MeOH and MeO_2CCF_3 or C(sp^2)-C(sp^3) coupled products involving a carbon atom of pincer ligands. DFT calculations were used to analyze the observed reactivity. It was concluded that the key factors favoring the C(sp^3)-O coupling are the *trans*-arrangement of the methyl ligand and the sulfonate group, the use of $CF_3CO_2^-$ as an O-nucleophile and DMSO as a solvent favoring the generation of highly electrophilic Pt^{IV}Me intermediates.

1. INTRODUCTION

The efficient incorporation of oxygen as an oxidant into Shilov-type chemistry (Scheme 1) has been a challenge for almost four decades,[1−3] and the advancements in this area of research continue to contribute to the field of catalytic CH functionalization.[4−9] Our recent efforts in the field of aerobic organoplatinum chemistry were focused on the development of mediator-free model systems featuring specifically designed facially chelating ligands as a tool to control the reactivity at a metal center.[7,10−13]

Recently, we have introduced Pt^{II} aqua complexes such as **1** (Scheme 2, *a*) supported by a sulfonated CNN pincer ligand

Scheme 1. Pt-Catalyzed Oxidative CH-Functionalization with O_2

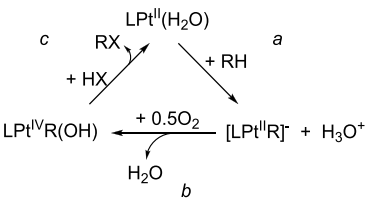

Received: July 25, 2022
Published: September 28, 2022

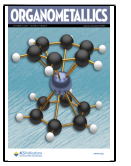

https://doi.org/10.1021/acs.organomet.2c00371
Organometallics 2022, 41, 2764−2783

Scheme 2. (a) Consecutive Arene CH Bond and O_2 Activation by (L1)$Pt^{II}(H_2O)$[11] and the (b) Inertness of (L)Pt^{IV}Ar(OH) in C−O Reductive Coupling[11,16]

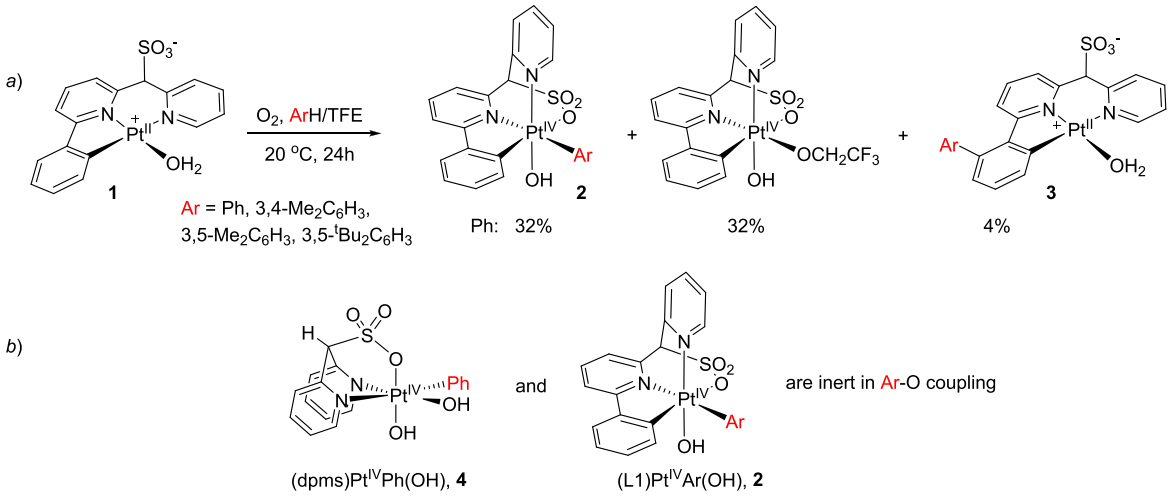

Scheme 3. C(sp^3)-X Coupling Reactivity of Pt^{IV}Me Complexes: (a) Reaction of (L1)Pt^{IV}Me(Y), 5a−5c, with O, S, and N Nucleophiles;[17] (b) Reaction of (dpms)$Pt^{IV}Me(OH)_2$, 6, with Water;[18,19] and (c) Pt^{IV}-to-Pt^{II} Methyl Transfer from (dpms)$Pt^{IV}Me(OH)_2$, 6, to (dpms)Pt^{II}Me(OH)[−26]

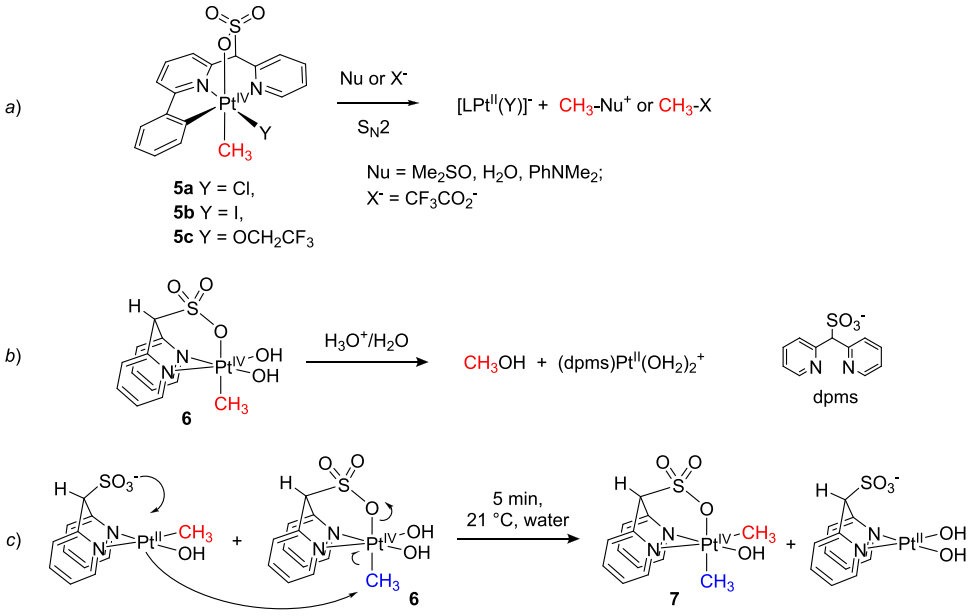

L1. These complexes are the active catalysts of H/D exchange between various arenes and TFE-d_1/D_2O (TFE = 2,2,2-trifluoroethanol) mixtures (compare with step *a*, Scheme 1).[10,14,15] Remarkably, when reacted with arenes ArH under an O_2 atmosphere, **1** produced arylplatinum(IV) derivatives **2** (compare with steps *a* and *b*, Scheme 1), along with formal products of their C−C coupling, **3**.[11]

On the downside, similar to arylplatinum(IV) complex (dpms)Pt^{IV}Ph(OH),[16] **4** (Scheme 2, *b*), supported by an earlier generation of sulfonated dipyridine ligands such as di(2-pyridyl)methanesulfonate (dpms), the resulting Pt(IV) aryl hydroxo complexes (L1)Pt^{IV}Ar(OH), **2**, are inert in C−O reductive elimination (compare with step *c*, Scheme 1). The lack of reactivity is not the case for analogous monomethylplatinum(IV) CNN-pincer complexes (L1)-Pt^{IV}Me(Y), **5a−5c**,[17] (Scheme 3, *a*) or a related (dpms)-$Pt^{IV}Me(OH)_2$, **6** (Scheme 3, *b*).[18,19] Similar to the results of prior studies of various platinum(IV) alkyls,[18−25] **5a−5c** can be engaged in C(sp^3)-X bond formation reactions (X = O, N, and S) that operate the S_N2 mechanism.[17]

Building on these results, one of the goals of this work was to find out if hydroxo complexes (L)Pt^{IV}Me(OH) (L = L1 and L2; Chart 1) can be generated aerobically (compare with step *b*, Scheme 1) from the corresponding precursors K[(L)-Pt^{II}Me], **8** and **9**.

Oxidation of dimethylplatinum(II) complexes stabilized by bidentate N,N-donors with O_2 in protic media is known to lead to dimethylhydroxoplatinum(IV) derivatives, but the corresponding monomethyl complexes do not react.[27] Monomethylplatinum(II) complexes can be engaged in oxidation with O_2 to form monomethylplatinum(IV) products when some carefully designed facially chelating ligands are employed such as dpms.[18,19,28]

https://doi.org/10.1021/acs.organomet.2c00371
Organometallics 2022, 41, 2764−2783

Chart 1. Monomethylplatinum(II) Complexes K[(L)Pt^{II}Me], 8 (L = L1) and 9 (L = L2), and Expected Products of Their Oxidation, Diastereomeric (L)Pt^{IV}Me(OH), 10a−10d (L = L1) and 11a−11d (L = L2), and Dimethylplatinum(IV) Products 12−12b (L = L1) and 13−13b (L = L2)

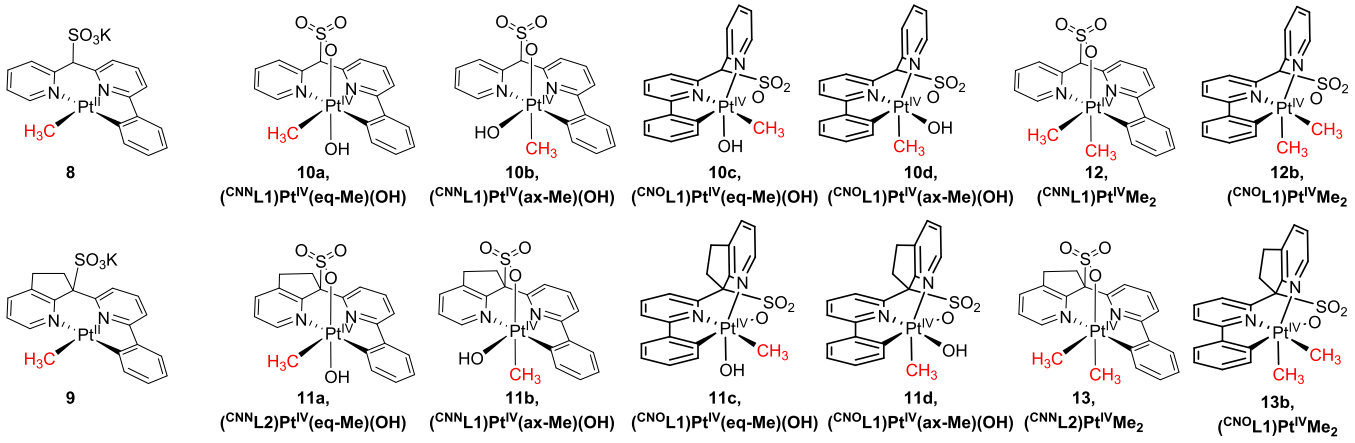

Scheme 4. Preparation of Complexes 8 and 9

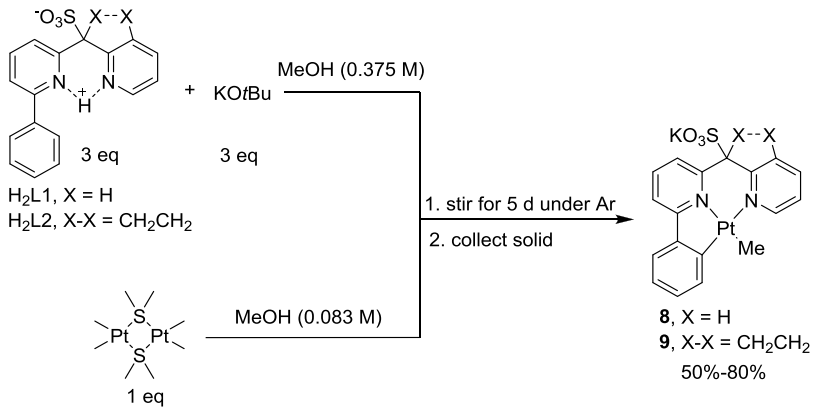

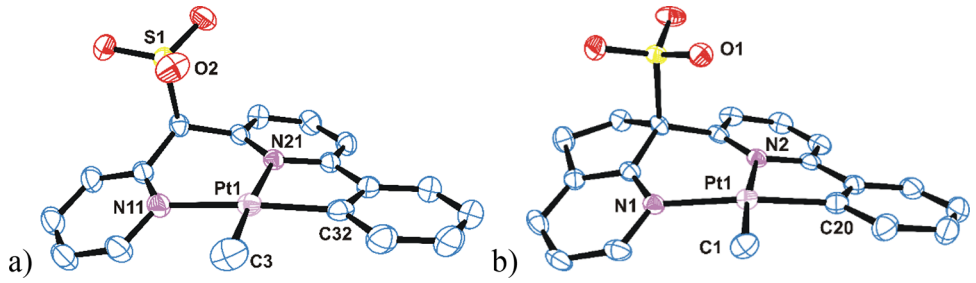

Figure 1. ORTEP drawing (50% probability ellipsoids) of (a) K[(L1)Pt^{II}Me], **8**, and (b) ^{n}Pr$_4$N[(L2)Pt^{II}Me], **9***. Cations, solvent molecules, and hydrogen atoms are omitted for clarity.

Four different diastereomeric complexes (L1)Pt^{IV}Me(OH), **10a−10d** (Chart 1), may result from oxidation of **8** that feature either CNN- (^{CNN}L1) or CNO- (^{CNO}L1) meridional arrangement of the three of four donor atoms of the sulfonated pincer ligand and have either axial or equatorial arrangement of the methyl ligand with respect to these triads of donor atoms. In addition, other Pt^{IV} products, dimethylplatinum(IV) complexes (^{CNN}L1)Pt^{IV}Me$_2$, **12**, and (^{CNO}L1)Pt^{IV}Me$_2$, **12b**, may result from oxidation of **8** as a result of an electrophilic Pt^{IV}-to-Pt^{II} methyl transfer from an initially formed (L1)-Pt^{IV}Me(OH) to the yet unreacted K[(L1)Pt^{II}Me]. Earlier, we observed a Pt^{IV}-to-Pt^{II} methyl transfer resulting in the formation of a C_1-symmetric dimethylplatinum(IV) complex (dpms)Pt^{IV}Me$_2$(OH), **7**, (Scheme 3, *c*).[26]

Remarkably, some "fine-tuning" of the reactivity of a Pt^{II} center in arene CH bond oxidative addition involving Pt^{II} complexes of sulfonated CNN-pincer ligands can be achieved by changing the rigidity of coordinated pincer ligands.[14] Accordingly, in this work, to affect the outcome of reactions of K[(L)Pt^{II}Me] and O_2, a modification of L was performed by incorporating a fused cyclopentane ring into L1, which resulted in its analog, L2.

With a variety of methylplatinum(IV) complexes (L)-Pt^{IV}Me(OH) expected from the oxidation of K[(L)Pt^{II}Me] (L = L1 and L2) with O_2, another goal of this work was to analyze the reactivity of (L)Pt^{IV}Me(OH) in C(sp^3)-X (X = O and C) reductive elimination as a function of their structure. The knowledge of factors that favor the formation of specific

https://doi.org/10.1021/acs.organomet.2c00371
Organometallics 2022, 41, 2764−2783

Scheme 5. Preparation of (L2)Pt^{IV}Me$_2$, 13

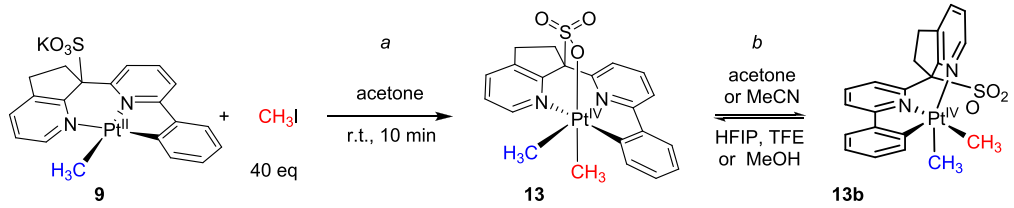

diastereomers (L)Pt^{IV}Me(OH) as well as the factors that affect their ability to produce C(sp^3)-O or C(sp^2)-C(sp^3) coupled products is critical for a successful development of aerobic CH functionalization reactions (Scheme 1) that utilize these or similar ligands. A discussion of the oxidation chemistry of **8** and **9** with O_2 and H_2O_2 and a discussion of the distinct C(sp^3)-X reductive elimination reactivity of the resulting methylplatinum(IV) derivatives are presented next.

2. RESULTS AND DISCUSSION

2.1. Preparation of K[(L1)Pt^{II}Me], 8, and K[(L2)Pt^{II}Me], 9. Complex K[(L1)Pt^{II}Me], **8**, was synthesized as reported previously[17] (Scheme 4). First, a potassium salt, K[HL1], was prepared by reacting H_2L1[17] with KO^{t}Bu dissolved in MeOH. The resulting solution was combined with a stirred suspension of $Pt_2Me_4(SMe_2)_2$ in MeOH. The solid dissolved and yellow target compound **8** started precipitating slowly from the mixture. After 5 days, **8** was isolated as a pure solid in 61% yield. The use of Na[HL1] salt in MeOH led to a lower isolated yield of Na[(L1)Pt^{II}Me] of 51% due to its faster methanolysis, leading to the formation of Na[(L1)Pt^{II}(OMe)] and methane.

X-ray quality crystals of **8** were produced by layering with Et_2O a saturated solution of **8** in MeOH/THF. The compound was characterized crystallographically (Figure 1a).

The same strategy was used for the preparation of K[(L2)Pt^{II}Me], **9**. Due to a lower solubility in MeOH, the product was isolated in a higher yield of 80%.

X-ray crystallographic characterization of the anionic methylplatinum(II) complex [(L2)Pt^{II}Me]$^-$ (Figure 1b) was performed for its salt with a ^{n}Pr$_4$N$^+$ counterion that was obtained using a salt metathesis of K[(L2)Pt^{II}Me] and [^{n}Pr$_4$N]Cl in acetone. ^{1}H NMR spectra of both **9** and [^{n}Pr$_4$N][(L2)-Pt^{II}Me], **9***, in DMSO-d_6 showed a methyl ligand signal at 1.00 ppm with a $^2J_{195PtH}$ coupling constant of 78 Hz. According to the crystallographic characterization, both **8** and **9*** feature a distorted square planar environment around a Pt^{II} center with the nitrogen atom of the terminal pyridine fragment forced below the plane defined by the metal, the attached aryl carbon atom, and the nitrogen atom of the central pyridine moiety of the pincer ligands. The distance between the plane and the terminal pyridine nitrogen was 0.317 Å for **8**, incorporating a more flexible pincer ligand L1 and 0.356 Å for **9*** containing a more rigid pincer ligand L2.

2.2. Preparation of (L1)Pt^{IV}Me$_2$, 12, and (L2)Pt^{IV}Me$_2$, 13. To facilitate the analysis of reaction mixtures produced in reactions **8** and **9** or **9*** with O_2, we prepared the anticipated (by)products (L)Pt^{IV}Me$_2$, **12** (L = L1)[17] and **13** (L = L2). Complex **13** was prepared following a procedure similar to the one published earlier for **12**[17] by reacting the corresponding K[(L)Pt^{II}Me] complex **9** dissolved in acetone with excess MeI (Scheme 5, *a*). The ^{1}H NMR spectra of **13** in 1,1,1,3,3,3-hexafluoropropan-2-ol (HFIP), TFE, or MeOH-d_4 solutions showed the presence of a single platinum complex with a Me:L2 ratio of 2:1. In particular, in TFE, the methyl ligands protons produced two singlets integrating as 3H each at 1.44 ppm ($^2J_{HPt}$ = 62 Hz) assigned to the equatorial CH$_3$ group located *trans* to the central pyridine moiety of L2 and at 1.14 ppm ($^2J_{HPt}$ = 80 Hz) assigned to the axial CH$_3$ group arranged *trans* to the sulfonate group. The assignment of the configuration of **13** in solutions was based on the analysis of the coupling constants $^2J_{195PtH}$ for the methyl ligand signals, as explained below.[17] An inspection of ^{1}H NMR parameters of diastereoisomers of methylplatinum(V) complexes explored earlier, (dpms)Pt^{IV}Me(OH)$_2$ and (dpms)Pt^{IV}Me$_2$(OH),[18] showed that methyl ligands situated *trans* to the SO$_3$ group had $^2J_{195PtH}$ values exceeding 75 Hz, whereas $^2J_{195PtH}$ < 70 Hz corresponded to the methyl groups *trans* to a pyridyl moiety. In addition, the configuration of a Pt^{IV} center in **13** dissolved in HFIP and TFE was confirmed by the selective NOE experiments (Figures S23 and S24).[29]

Notably, similar to **12**,[17] complex **13** can undergo a facile isomerization in solutions to produce a diastereomer, (^{CNO}L2)Pt^{IV}Me$_2$, **13b** (Scheme 5, *b*). The isomerization involves a departure of the sulfonate group from a Pt^{IV} center and a concerted rotation of the Pt^{IV}Me$_2$ fragment such that one of the methyl ligands assumes an axial position opened as a result of the departure of the sulfonate. Complex **13b** was detected by ^{1}H NMR spectroscopy in acetone and MeCN. When a sample of solid **13** was dissolved in acetone-d_6 or CH$_3$CN-d_3, the **13**:**13b** ratio was 1:0.83 or 1:0.4, respectively. As an example, in acetone-d_6 solutions containing both **13** and **13b**, four signals of methyl group protons were detected at 1.40 ppm ($^2J_{195PtH}$ = 65 Hz), 1.25 ppm ($^2J_{195PtH}$ = 65 Hz), 0.96 ppm ($^2J_{195PtH}$ = 80 Hz), and 0.85 ppm ($^2J_{195PtH}$ = 69 Hz). Based on the $^2J_{195PtH}$ coupling constants values, the signal at 0.96 ppm ($^2J_{195PtH}$ = 80 Hz) was assigned to the methyl ligand in complex **13** where it is arranged *trans* to the SO$_3$ group and the signal of a matching integral intensity at 1.40 ppm ($^2J_{195PtH}$ = 65 Hz) to the methyl ligand of **13** located *trans* to the central pyridine moiety of L2. The remaining two signals of equal intensity at 1.25 ppm ($^2J_{195PtH}$ = 65 Hz) and 0.85 ppm ($^2J_{195PtH}$ = 69 Hz) were assigned to **13b**. A facile isomerization of trihydrocarbylplatinum(IV) species was reported earlier.[30−32]

Single crystals of **13** were grown from its solution in TFE by allowing the solvent to slowly evaporate. Similarly were grown single crystals of **12** whose solid-state structure was not reported earlier. The crystal structures of **12** and **13** are shown in Figure 2. In both cases, the sulfonated pincer ligands adapt a meridional CNN arrangement of three of their donor atoms. Comparing the Pt−O(SO$_2$) distances in complexes **12** and **13**, it is worth noting that the Pt−O distance in complex **13**, 2.278 Å, is 0.014(6) Å longer as compared to complex **12** (2.264 Å). In turn, in a methoxy-analog of complex **6** (Scheme 3, *c*), (dpms)Pt^{IV}(axial-Me)(OH)(OMe), containing an unstrained dpms ligand, the Pt−O(SO$_2$) bond is only 2.225(5) Å long.[19]

https://doi.org/10.1021/acs.organomet.2c00371
Organometallics 2022, 41, 2764−2783

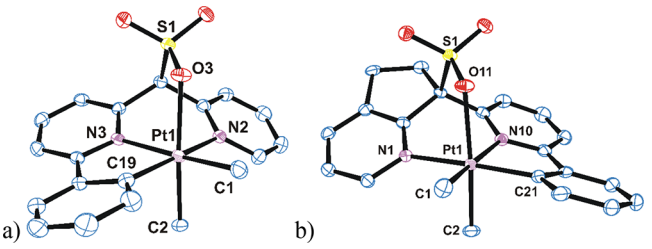

Figure 2. ORTEP drawing (50% probability ellipsoids) of (a) (L1)$Pt^{IV}Me_2$, **12**. Selected bond lengths (Å): Pt1-O3, 2.264(3), Pt1-N2, 2.153(3), Pt1-N3, 2.094(3), Pt1-C19, 2.012(4), Pt1-C2, and 2.046(4). (b) (L2)$Pt^{IV}Me_2$, **13**. Selected bond lengths (Å): Pt1-O11, 2.278(3), Pt1-N1, 2.142(3), Pt1-N10, 2.097(3), Pt1-C21, 2.007(3), Pt1-C2, and 2.040(4). Solvent molecules and hydrogen atoms are omitted for clarity.

Based on these observations, we presume that (L1)$Pt^{IV}Me_2$, **12**, features a somewhat stronger stabilization of a Pt^{IV} center by the SO_3^- group than **13** does. Accordingly, due to a slightly better SO_3^- group accessibility, $[(L1)Pt^{II}Me]^-$ may be somewhat more nucleophilic than $[(L2)Pt^{II}Me]^-$, favoring faster and more competitive rates of formation of $(L)Pt^{IV}Me_2$ (compare with Scheme 3, *c*).

2.3. Oxidation of K[(L)Pt^{II}Me] Using H_2O_2. Oxidation of **8** and **9** with H_2O_2 was carried out with the goal to compare their products with those from aerobic oxidation (Scheme 6). In fact, reactions with H_2O_2 resulted in easier-to-identify compounds.

*2.3.1. Oxidation of K[(L2)Pt^{II}Me], **9**, with H_2O_2: Formation of **11c** and **15**.* Reaction of K[(L2)Pt^{II}Me], **9**, dissolved in acetone with 5 equiv of H_2O_2 used as a 30% aqueous solution (Scheme 6, *d*) led to a rapid disappearance of the original yellow/green color of **9**. After 30 min, a crystalline solid identified as (^{CNO}L2)Pt^{IV}(eq-Me)(OH), **11c**, precipitated from the mixture and was isolated in a pure form in 37% yield. Additional amounts of complex **11c** precipitated from the filtrate that was left to stand for a few hours.

Single crystals of **11c** suitable for X-ray diffraction characterization were produced by crystallization of **11c** from acetone or methanol solutions. When standing of the original reaction mixture was extended to 2−5 days, crystals of another product, **15** (Scheme 6, *e* and *f*), co-precipitated along with **11c** in a 1:2 molar ratio, as determined by ^{1}H NMR. The byproduct **15** was identified by X-ray diffraction as a dinuclear bis-hydroxo-bridged methylplatinum(IV) complex in which the sulfonate groups are not coordinated to the metal. Complex **15** can be viewed as a product of dimerization of **11b** involving a displacement of a weakly coordinated sulfonate ligand in one moiety of **11b** with a hydroxo ligand of another molecule of **11b**. Notably, **11b** was not observed in our reaction mixtures. Our attempts to separate **15** from **11c** using crystallization from various solvents were not successful.

The crystal structure of **11c** is shown in Figure 3a. In **11c**, a Pt^{IV} center has a distorted octahedral geometry. The pincer ligand adapts a meridional CNO-arrangement of three of its four donor atoms, and the methyl ligand occupies an equatorial position. An analysis of the solid-state structure of **11c** shows a 2.101 Å long Pt1-N1 bond trans to the methyl and 2.053 Å long Pt1-N3 bond trans to the hydroxo ligand. The Pt1-N1 bond is longer due to a stronger *trans*-influence of the methyl as compared to that of the hydroxo ligand. Similarly, a strong *trans*-influence of the aryl group and, potentially, some pincer ligand strain may be responsible for some elongation of the Pt1-O2 bond (2.201 Å) involving a sulfonate group oxygen atom. To compare, the length of the Pt1-O1 bond involving an oxygen atom of a hydroxo ligand *trans* to a terminal pyridine group is only 1.969 Å.

Similarly, in the dinuclear complex **15**, a Pt-O1 bond trans to the methyl ligand is elongated (2.195 Å), as compared to a Pt-O1′ bond (2.013 Å) situated *trans* to the pincer ligand's central pyridine fragment. Also elongated is a Pt1-N25 bond (2.155 Å) located *trans* to the aryl fragment of the pincer ligand, as compared to a Pt1-N22 bond (2.035 Å), which is *trans* to the equatorial hydroxo ligand.

Complex **11c** was characterized in DMSO and HFIP solutions by means of ^{1}H and ^{13}C NMR spectroscopy, selective 1D difference NOE experiments, and electrospray ionization mass-spectrometry (ESI-MS). A ^{1}H NMR spectrum of **11c** in DMSO-d_6 exhibited a singlet of the methyl ligand protons at 0.53 ppm ($^2J_{HPt}$ = 64 Hz) with ^{195}Pt-satellites integrating as 3H and a characteristic broad singlet at 5.25 ppm assigned to a Pt^{IV}-bound hydroxo ligand proton integrating as 1H. The signal at 5.25 ppm disappeared upon addition of a drop of D_2O due to a virtually complete H/D exchange in the hydroxo ligand, confirming the signal's assignment to the

Scheme 6. Products of Oxidation of K[(L)Pt^{II}Me], 8 (L = L1), and 9 (L = L2), with H_2O_2

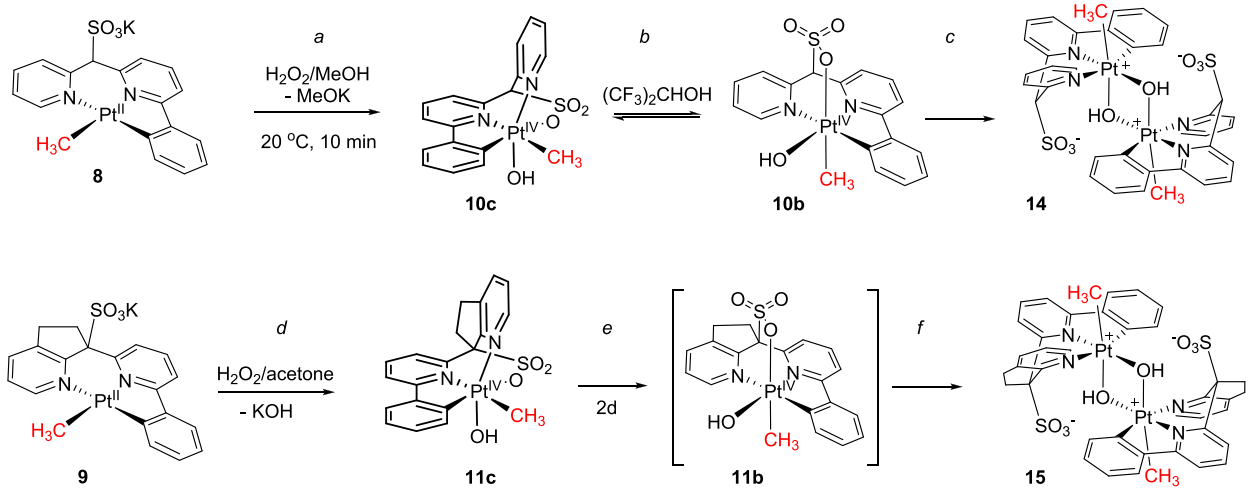

https://doi.org/10.1021/acs.organomet.2c00371
Organometallics 2022, 41, 2764−2783

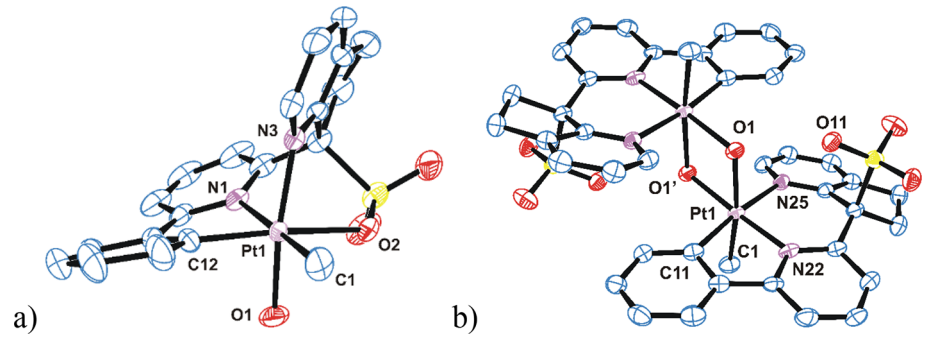

Figure 3. ORTEP drawing (50% probability ellipsoids) of (a) (^{CNO}L2)Pt^{IV}(eq-Me)OH, **11c**. Selected bond lengths (Å): (a) Pt1-N3, 2.053(3), Pt1-N1, 2.101(3), Pt1-C12(4), 1.993, P1-C1, 2.043(4), Pt1-O1, 1.969(3), Pt1-O2, and 2.201(2). (b) (^{CNN}L2)$_2$Pt$^{IV}_2$(ax-Me)$_2$(μ-OH)$_2$, **15**. Selected bond lengths (Å): Pt1-O1, 2.195(3), Pt1-O1′, 2.013(3), Pt1-N22, 2.035(4), Pt1-N25, 2.155(4), Pt1-C1, 2.046(4), Pt1-C11, and 2.005(5). Solvent molecules and hydrogen atoms are omitted for clarity.

Scheme 7. Plausible Mechanism for the Oxidation of K[(L2)Pt^{II}Me], 9, with H_2O_2 in Acetone (Numbers in Blue Correspond to the Relative Reaction Gibbs Energies, ΔG°_{298}, in kcal/mol (PBE-D3/LACVP/PBF(acetone)//PBE/LACVP** Level of Theory))**

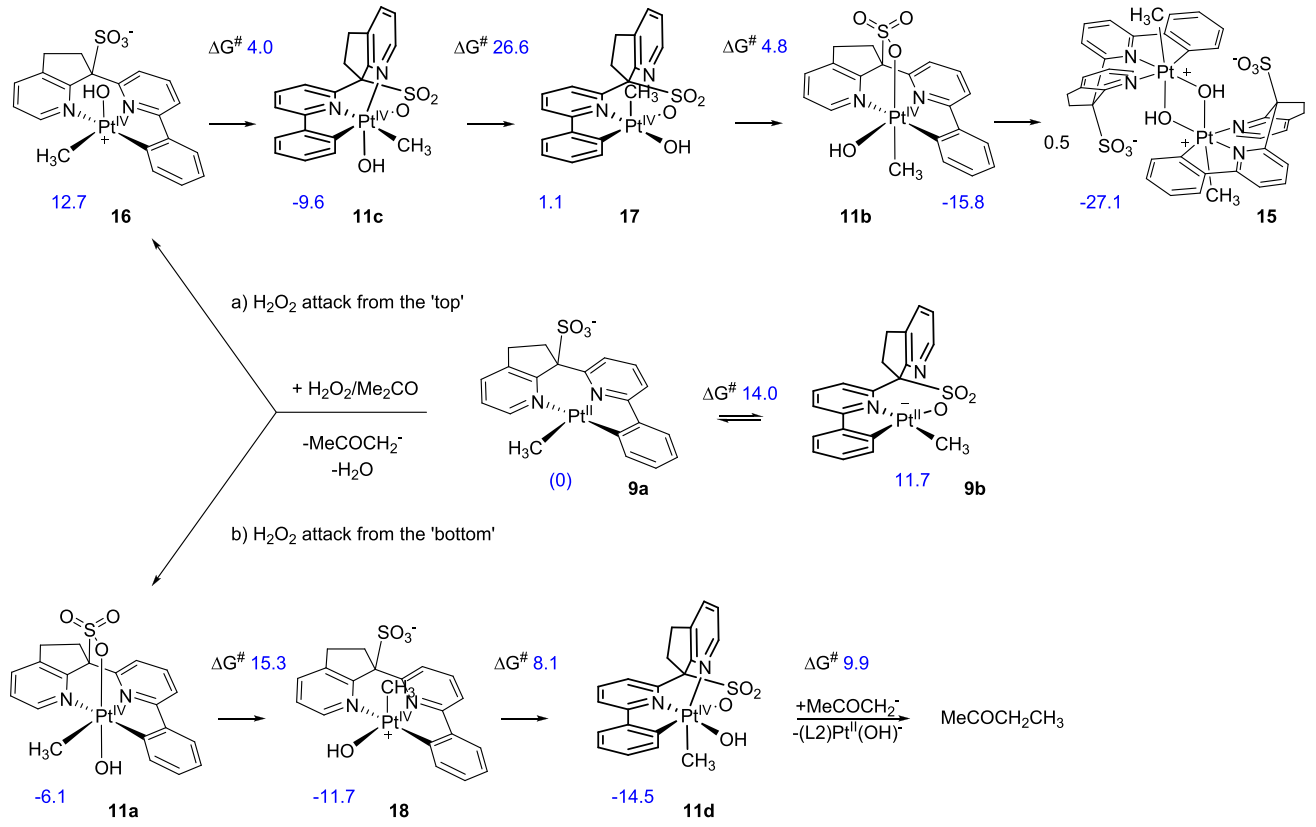

hydroxo ligand proton. The value of the methyl group coupling constant, $^2J_{195PtH}$ = 64 Hz, corresponds to a *trans*-arrangement of the methyl with respect to the nitrogen atom of a pyridine fragment.[17] Using selective NOE experiments, it was shown that in DMSO solutions **11c** retained the same configuration as in the solid state (Figure S19).[29] The ESI-MS(+) spectrum of **11c** dissolved in HFIP containing a KPF_6 additive exhibited a strong signal assigned to a [**11c** + K]$^+$ ion.

Due to a poor solubility of **15** in the most common solvents and a better solubility in HFIP, its ^{1}H NMR spectrum was acquired in HFIP. The spectrum exhibited a methyl group signal at 2.05 ppm integrating as 6H with the $^2J_{195PtH}$ value of 58 Hz. The small $^2J_{195PtH}$ value suggests that the methyl and the SO_3 group are not mutually *trans* and, therefore, dissociation of **15** to form a "monomer" **11b** did not occur in HFIP. A signal of OH groups of **15** was, presumably, buried under the solvent peaks and was not observed.

2.3.2. Plausible Mechanism of Formation of 11c and 15 (DFT). A plausible mechanism of the formation of **11c** and **15** from K[(L2)Pt^{II}Me] and H_2O_2 in acetone solutions, supported by our DFT calculations, is shown in Scheme 7. The organometallic anion present in **9**, [(^{CNN}L2)Pt^{II}Me]$^-$, **9a**, can undergo an isomerization to form [(^{CNO}L2)Pt^{II}Me]$^-$, **9b**, having a meridional CNO-arrangement of the pincer ligand donor atoms. A DFT-calculated Gibbs energy of the isomerization reaction in acetone solutions, ΔG°_{298}, is +11.7 kcal/mol, and the Gibbs activation energy is 14.0 kcal/mol. Taking into account a much lower Gibbs activation energy of

https://doi.org/10.1021/acs.organomet.2c00371
Organometallics 2022, 41, 2764−2783

reactions of H_2O_2 with $[(^{CNN}L2)Pt^{II}Me]^-$, **9a**, (*vide infra*), one can neglect any possible involvement of **9b** in the oxidation.

An electrophilic attack of H_2O_2 at a highly nucleophilic Pt^{II} center of $[(^{CNN}L2)Pt^{II}Me]^-$ anion **9a** is facilitated by protic components of the reaction mixture (water or H_2O_2) and can occur from the "top" of the metal coordination plane, as shown in Scheme 7, *a*, or from the "bottom" (Scheme 7, *b*). In both cases, the reaction is expected to be very fast. Our estimate of the Gibbs activation energy for the reaction in methanol modeling the proton donor environment in our reaction mixtures due to H_2O_2 and H_2O is 5.9 kcal/mol for the attack from the top and even lower for the attack from the bottom. These values are close to or even less than the Gibbs activation energy of a diffusion-controlled bimolecular process in acetone of about 6 kcal/mol at 293 K.[29] Hence, both reaction directions in Scheme 7, *a* and *b*, are likely to be diffusion-controlled and, therefore, are almost equally fast. Expectedly, all available **9** is consumed rapidly so that unreacted **9** cannot participate in subsequent Pt^{IV}-to-Pt^{II} methyl transfer reactions with $(L2)Pt^{IV}Me(OH)$ species (compare to a reaction in Scheme 3, *c*). This consideration allows one to account for the absence of $(L2)Pt^{IV}Me_2$, **13**, among reaction products. The attacks from two opposite sides of a Pt^{II} coordination plane might lead to all four possible diastereoisomers $(L2)Pt^{IV}Me(OH)$, as discussed next.

An attack of H_2O_2 at a Pt^{II} center in **9a** from the top is expected to produce a 5-coordinate Pt^{IV} transient **16** that can rapidly ($\Delta G_{298}^{\#}$ = 4.0 kcal/mol) isomerize to form complex **11c** (Scheme 7, *a*). Complex **11c** is expected to be relatively stable kinetically. The Gibbs activation energy for isomerization of **11c** into a highly reactive electrophilic methylplatinum(IV) species **17** is moderately high, $\Delta G_{298}^{\#}$ = 26.6 kcal/mol. Accordingly, **11c** could be isolated from the actual reaction mixtures. In turn, **17** is calculated to react rapidly, with the Gibbs activation energy $\Delta G_{298}^{\#}$ = 4.8 kcal/mol, to form a more stable diastereomer **11b**. Finally, complex **11b** can dimerize in an exergonic reaction to produce **15**. In fact, **15** was observed to slowly crystallize from reaction mixtures in the course of a few days.

An attack of H_2O_2 at a Pt^{II} center from the bottom of the metal coordination unit in **9a** is expected to result in **11a** (Scheme 7, *b*). The latter is calculated to produce a 5-coordinate transient **18** at a fast enough rate ($\Delta G_{298}^{\#}$ = 15.3 kcal/mol) in an exergonic reaction. In turn, the Gibbs activation energy, ΔG°_{298}, for the isomerization of **18** to form a more stable complex **11d** is very low, only 8.1 kcal/mol. Finally, **11d** may be consumed in anticipated reactions with strong nucleophiles present in the solution, for instance, acetone-derived enolate anions. The calculated Gibbs activation energy for the latter reaction is only 9.9 kcal/mol. As such, some products of a Pt^{IV}-to-a nucleophile methyl transfer might form as a result of the realization of the reaction path *b* in Scheme 7. Our attempts to detect these products in reaction mixtures by means of ^{1}H NMR spectroscopy were not successful.

In summary, as opposed to the attack of H_2O_2 at a Pt^{II} center in **9a** from the top that resulted in two isolable products, **11c** and **15**, an attack from the bottom of **9a** is not expected to result in Pt^{IV} complexes that are stable enough under the reaction conditions employed.

*2.3.3. Oxidation of K[(L1)Pt^{II}Me], **8**, with H_2O_2 - Formation of **10c** and **14**.* By reacting $K[(L1)Pt^{II}Me]$, **8**, with 5 equiv of 30% aqueous H_2O_2 dissolved in MeOH, a white solid assigned the structure of **10c** (*vide infra*) was produced in 10 min. The product was isolated in 63% yield and was pure by ^{1}H NMR spectroscopy (Scheme 6, *a*). The structure of the product was assigned using the characterization details provided below and an analogy with the oxidation of **9** with H_2O_2 resulting in isolable and well-characterized **11c**. Complex **10c** was only barely soluble in the most common solvents including MeOH, TFE, DMSO, and water, but it had a higher solubility in HFIP. A ^{1}H NMR spectrum of **10c** in DMSO-d_6 showed a methyl ligand singlet at 0.53 ppm integrating as 3H with a $^2J_{195PtH}$ value of 67 Hz, suggesting that the methyl ligand is *trans* to a pyridine nitrogen atom.[17] A broad singlet at 5.40 ppm was assigned to a proton of a hydroxo ligand. This signal disappeared once a drop of D_2O was added to the solution due to a facile H/D exchange. ESI-MS(+) characterization of HFIP solutions of **10c** allowed one to observe the signal of a protonated species, **10c**·H^+, with an expected isotopic distribution.

Interestingly, when **10c** was dissolved in HFIP, a ^{1}H NMR spectrum of the resulting solution showed the presence of one more methylplatinum(IV) species with the methyl group signal at 1.73 ppm and a $^2J_{195PtH}$ value of 76 Hz in a 1:2 molar ratio to **10c**. Based on a $^2J_{195PtH}$ value of 76 Hz, we presume that the methyl ligand in the new species is *trans* to the sulfonate group and we hypothesize that the species producing this signal is **10b** (Scheme 6, *b*). By layering the resulting HFIP solution containing both methylplatinum(IV) complexes with diethyl ether, a compound was crystallized, which was identified by single-crystal X-ray diffraction as **14** (Scheme 6, *c*, and Figure 4), a formal product of dimerization of **10b**. The structural parameters of **14** (Figure 4) resemble closely those of **15** (Figure 3b).

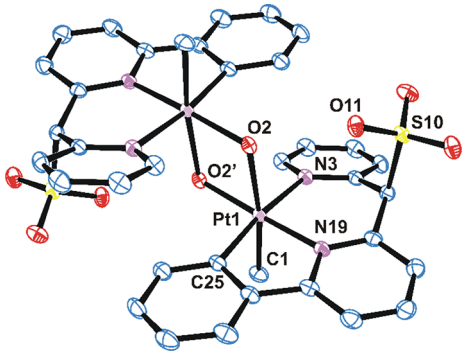

Figure 4. ORTEP drawing (50% probability ellipsoids) of $(^{CNN}L1)_2Pt^{IV}_2(ax\text{-}Me)_2(\mu\text{-}OH)_2$, **14**. Solvent molecules and hydrogen atoms are omitted for clarity. Selected bond lengths (Å): Pt1-O2, 2.209(2), Pt1-O2′, 2.004(2), Pt1-N19, 2.020(2), Pt1-N3, 2.170(2), Pt1-C1, 2.053(3), Pt1-C25, and 2.000(3).

Hence, not unexpectedly, there is much similarity in the oxidation of $K[(L)Pt^{II}Me]$ complexes, **8** (L = L1) and **9** (L = L2), with H_2O_2 that involves formation of isolable methylplatinum(IV) species $(^{CNO}L)Pt^{IV}(eq\text{-}Me)OH$, **10c** (presumed) and **11c**, as well as dinuclear complexes $(^{CNN}L)_2Pt^{IV}_2(ax\text{-}Me)_2(\mu\text{-}OH)_2$, **14** and **15** (Scheme 6). In spite of this similarity, it appears that $(^{CNO}L1)Pt^{IV}(eq\text{-}Me)(OH)$, **10c**, is less kinetically stable than its analog $(^{CNO}L2)Pt^{IV}(eq\text{-}Me)(OH)$, **11c**. This difference was manifested in a fast isomerization of **10c** to **10b** that was observed in HFIP solutions with a subsequent dimerization of **10b**

https://doi.org/10.1021/acs.organomet.2c00371
Organometallics 2022, 41, 2764−2783

Scheme 8. Products of Oxidation of K[(L)Pt^{II}Me], 8 (L = L1), and 9 (L = L2), with O_2 in MeOH

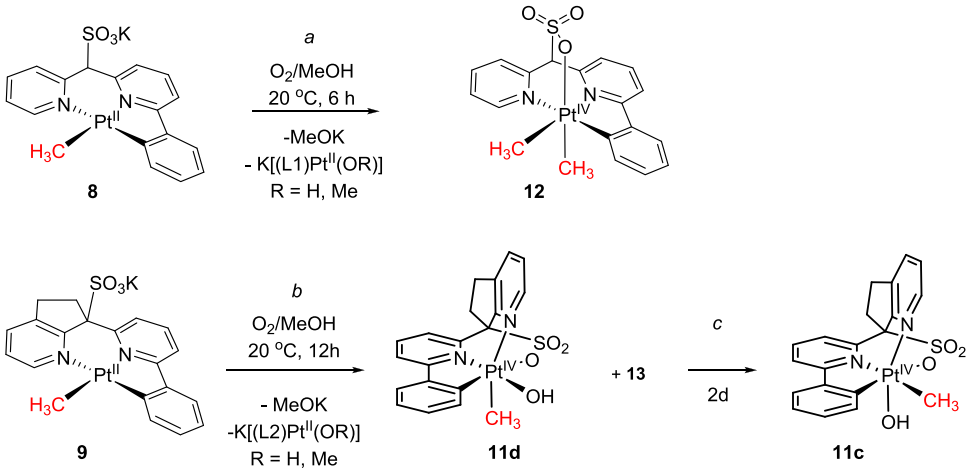

Scheme 9. Pausible Mechanism for the Oxidation of K[(L1)Pt^{II}Me], 8, with O_2 in MeOH (Numbers in Blue Correspond to the Relative Reaction Gibbs Energies, $\Delta G°_{298}$, in kcal/mol (PBE-D3/LACVP/PBF(MeOH)//PBE/LACVP** Level of Theory))**

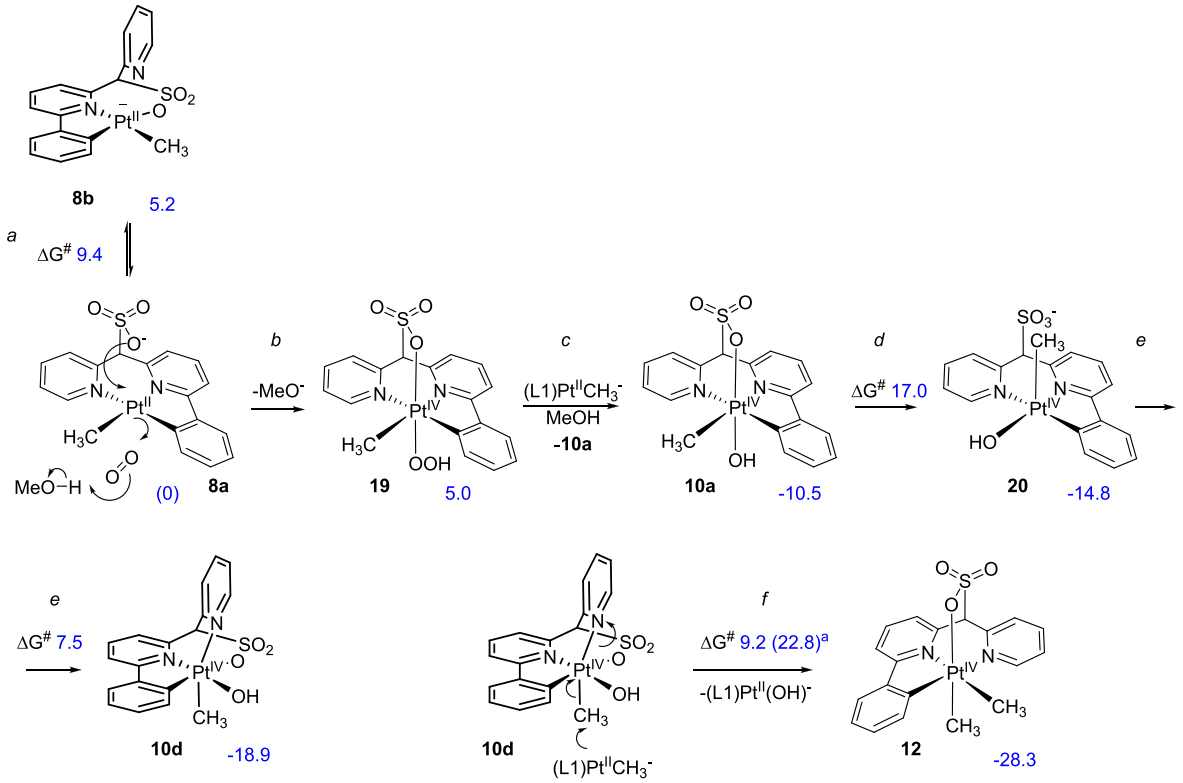

[a]Without a dispersion correction; PBE/LACVP**/PBF(MeOH)//PBE/LACVP** level of theory.

leading to a dinuclear product (^{CNN}L1)$_2$Pt$^{IV}_2$(ax-Me)$_2$(μ-OH)$_2$, **14**. In the case of (^{CNO}L2)Pt^{IV}(eq-Me)(OH), **11c**, a similar reaction sequence to produce **15** required a few days. Accordingly, our computational analysis suggests that **10c** is expected to undergo isomerization to **10b** at a rate about 20 times faster ($\Delta G_{298}^{\#}$ = 24.8 kcal/mol) than the rate of isomerization of **11c** to **11b** ($\Delta G_{298}^{\#}$ = 26.6 kcal/mol for **11c**; see Scheme 7, path *a*).

2.4. Oxidation of K[(L)Pt^{II}Me] Using O_2. Oxidation of K[(L)Pt^{II}Me] with O_2 in MeOH led to Pt(IV) methyl complexes whose structure was dependent on the pincer ligand L used. The results are summarized in Scheme 8.

2.4.1. Oxidation of K[(L1)Pt^{II}Me], 8, with O_2 in MeOH. Stirring solution of K[(L1)Pt^{II}Me], **8**, in MeOH under 1 atm of O_2 for 6 h resulted in the formation of a single methylplatinum(IV) product, a dimethyl complex (L1)-Pt^{IV}Me$_2$, **12**, that precipitated from the reaction mixture and was isolated in 95% yield as a pure solid, along with byproducts K[(L1)Pt^{II}(OR)] where R = H or Me (Scheme 8, *a*). The byproducts K[(L1)Pt^{II}(OR)] were detected in the solution by means of ^{1}H NMR spectroscopy (Figure S29) and ESI-MS spectrometry. Compared to oxidation of **8** with H_2O_2, the aerobic oxidation reaction was much slower so that the expected primary products, monomethylplatinum(IV) species,

https://doi.org/10.1021/acs.organomet.2c00371
Organometallics 2022, 41, 2764−2783

were able to react with yet remaining **8** (Pt^{IV}-to-Pt^{II} methyl transfer) to form **12**, as described next.

*2.4.2. Plausible Mechanism of Aerobic Oxidation of K[(L1)Pt^{II}Me], **8**, with O_2 in MeOH and Formation of **12** (DFT).* A plausible mechanism of the title reaction supported by our DFT calculations is shown in Scheme 9. The anion present in the solid **8**, $[(^{CNN}L1)Pt^{II}Me]^-$, **8a**, in solutions can produce an isomer $[(^{CNO}L1)Pt^{II}Me]^-$, **8b**, having a meridional CNO-arrangement of the pincer ligand donor atoms (Scheme 9, *a*). A DFT-calculated Gibbs energy of the isomerization reaction in MeOH solutions, ΔG°_{298}, is +5.2 kcal/mol, and the Gibbs activation energy for this process is 9.4 kcal/mol. In the following analysis, we assume that the reaction of **8** with O_2 involves predominantly the more stable anion **8a** that is attacked by O_2 from the bottom (Scheme 9, *b*) as it was proposed for an analogous reaction of $[(dpms)Pt^{II}Me(OH)]^-$ with O_2 in water.[33]

A reaction of the anion $[(^{CNN}L1)Pt^{II}Me]^-$, **8a**, with O_2 in MeOH is assisted with a proton transfer from the solvent and leads to the formation of a hydroperoxoplatinum(IV) intermediate **19**; the reaction is slightly, by +5.0 kcal/mol, endergonic (Scheme 9, *b*). As a result of a nucleophilic attack at the hydroperoxo ligand of **19** by another equivalent of **8a**, 2 equiv of hydroxoplatinum(IV) complex **10a** is produced in an overall exergonic step (Scheme 9, *c*). Due to a strong *trans*-influence of the methyl ligand, **10a** is destabilized and undergoes a relatively facile ($\Delta G_{298}^{\#}$ = 17.0 kcal/mol) isomerization to form a five-coordinate intermediate **20** where the unfavorable methyl ligand interaction is eliminated (Scheme 9, *d*). This step is predicted to be slightly exergonic. The isomerization involves a departure of the sulfonate group from a Pt^{IV} center and a concerted "rotation" of the $Pt^{IV}Me(OH)$ fragment with the methyl ligand moving toward the dissociating sulfonate. The reactive 5-coordinate transient **20** can next be engaged in a rapid ($\Delta G_{298}^{\#}$ = 7.5 kcal/mol) isomerization to form a methylplatinum(IV) complex **10d** (Scheme 9, *e*). Finally, **10d** is electrophilic enough and can be attacked by yet unreacted **8a** acting as a nucleophile and engaged in a Pt^{IV}-to-Pt^{II} methyl transfer to produce $(L1)Pt^{IV}Me_2$ and $K[(L1)Pt^{II}(OH)]$ (Scheme 9, *f*). The latter byproduct can react with MeOH to form $K[(L1)Pt^{II}(OMe)]$. A combination of a noticeable electrophilicity of **10d** and a high nucleophilicity of **8a** results in a complete conversion of **10d** to **12** (Scheme 9, *f*). A DFT-calculated Gibbs activation energy for step *f* is 9.2 kcal/mol with an applied dispersion energy correction (PBE-D3 functional), as for all other steps in Scheme 9. It is possible that the PBE-D3 functional overestimates the dispersion energy contribution to this activation energy to some extent; without such correction, the $\Delta G_{298}^{\#}$ is higher, 22.8 kcal/mol.

*2.4.3. Oxidation of K[(L2)Pt^{II}Me], **9**, with O_2 in MeOH Solutions.* Solutions of $K[(L2)Pt^{II}Me]$, **9**, in aprotic acetone stirred under 1 atm pressure of O_2 did not change in the course of a few days but in MeOH, oxidation of **9** with O_2 was complete in 12 h (Scheme 8, *b*). The oxidation of **9** was slower than that of **8** under the same conditions. Upon completion of the reaction, two methylplatinum products were identified by ^{1}H NMR spectroscopy in the resulting solution (NMR yields are given in parentheses), a dimethylplatinum(IV) complex $(L2)Pt^{IV}Me_2$, **13** (12%), and a methylplatinum(IV) complex $(L2)Pt^{IV}Me(OH)$ assigned as **11d** (31%), along with a mixture of byproducts $K[(L2)Pt^{II}(OR)]$ (R = H and Me) identified by ^{1}H NMR spectroscopy and ESI-MS(−). The oxidation reaction was accompanied with a partial protonolysis of **9** and formation of methane, which accounted for about 50% of all consumed complex **9**. Remarkably, in the reaction of **9** with O_2 complex $(L2)Pt^{IV}Me_2$, **13**, formed as a minor byproduct only, as opposed to the analogous reaction of **8** with O_2, where $(L1)Pt^{IV}Me_2$, **12**, was the only observed Pt^{IV} species. Given a bimolecular nature of Pt^{IV}-to-Pt^{II} methyl transfer,[26] this undesirable reaction may become unobservable in the corresponding hypothetical catalytic systems for methane functionalization where the concentration of $[(L)Pt^{II}Me]^-$ species is expected to be very low.

Complex **11d** present in the reaction mixture above exhibited a signal of a terminal pyridyl *ortho*-hydrogen atom at 9.55 ppm and a singlet of methyl ligand at 1.49 ppm with a coupling constant $^2J_{195PtH}$ value of 71 Hz typical for a *trans*-coordinated pyridine fragment. The mutual arrangement in space of the methyl ligand, the terminal pyridine fragment of the pincer ligand L2 and its phenylene fragment that is expected for **11d**, was confirmed using selective 1D-difference NOE experiments (Figure S20).[29] Analysis of reaction mixtures by means of ESI mass spectroscopy showed the presence of a strong signal of an adduct $(L2)Pt^{IV}Me(OH)\cdot K^+$ with a proper isotopic distribution. The product **11d** was stable in methanolic solution for a few hours only and decomposed upon an attempted isolation. When the reaction mixture was left to stand for 2 days, **11d** disappeared and a precipitate formed that was identified by NMR spectroscopy as **11c** (Scheme 8, *c*). Our attempts to modify the reaction conditions and increase the yield of **11d** were not successful. Running an aerobic oxidation of a more methanol-soluble tetra-*n*-propylammonium salt, $^nPr_4N[(L2)Pt^{II}Me]$, **9***, at a higher concentration, led to the same products but in lower yields, 5% for **13** and 26% for **11d**, with increased fractions of byproducts $K[(L2)Pt^{II}(OR)]$ (R = H and Me). When the oxidation was performed using a suspension of **9** in MeOH, the same set of products was observed as well with **11d** being the major methylplatinum(IV) species and the NMR yield of **11d** being still ∼30%.

*2.4.4. Plausible Mechanism of Oxidation of K[(L2)Pt^{II}Me], **9**, with O_2 in MeOH and Formation of **11d** (DFT).* A plausible mechanism of oxidation of $K[(L2)Pt^{II}Me]$, **9**, with O_2 in MeOH solutions supported by our DFT calculations is given in Scheme S1; it is similar to the one in Scheme 9 for the oxidation of $K[(L1)Pt^{II}Me]$, **8**. The most noticeable difference is seen when the Gibbs energies are compared for individual reaction steps *b*, *d*, *e*, and *f* in both schemes. These steps include either coordination (*b* and *e*) or dissociation (*d*) of the SO_3^- group to/from a Pt^{IV} center. The energy change for steps *b* and *e* that include coordination of the SO_3^- group to a Pt^{IV} center is 1.2−2.5 kcal/mol less exergonic for derivatives of ligand L2 (Scheme S1) than for the ligand L1-supported complexes (Scheme 9). In turn, the energy change for step *d* that includes dissociation of the SO_3^- group from a Pt^{IV} center is 1.2 kcal/mol less endergonic for L2 derivatives. These differences suggest that the more rigid ligand L2 does not stabilize a Pt^{IV} center as strongly as a more flexible ligand L1 can. Interestingly, the nucleophilicity of $[(L)Pt^{II}Me]^-$ species is also affected by the identity of a pincer ligand. A comparison of the Gibbs activation energies for a Pt^{IV}-to-Pt^{II} methyl transfer step *f* in Scheme 9 and Scheme S1 shows that $\Delta G_{298}^{\#}$ is noticeably, by 3.6−4.4 kcal/mol, higher for the reaction involving **9a**. For step *f*, the $\Delta G_{298}^{\#}$ value in Scheme S1 is 12.8 kcal/mol, 3.6 kcal/mol higher than in Scheme 9, with the

https://doi.org/10.1021/acs.organomet.2c00371
Organometallics 2022, 41, 2764−2783

Scheme 10. Aerobic Oxidation of K[(L2)Pt^{II}Me], 9, in an Acetone-d_6–TFE mixture (Numbers in Blue Correspond to the Relative Reaction Gibbs Energies in kcal/mol (PBE-D3/LACVP/PBF(Me_2CO)//PBE/LACVP** Level of Theory))**

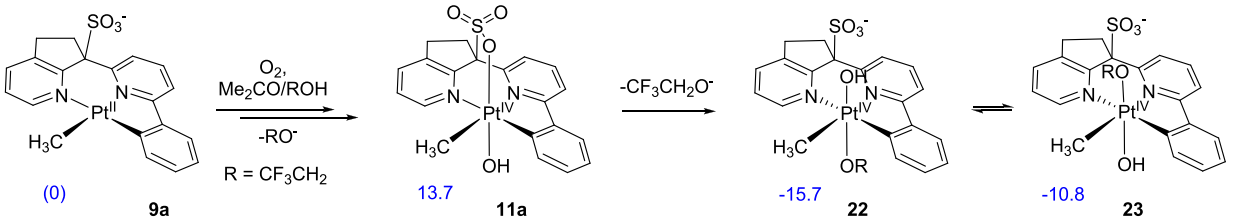

dispersion correction applied (as for all other energy values) and it is 27.2 kcal/mol, 4.4 kcal/mol higher than in Scheme 9, without such correction. Hence, complex [(L1)Pt^{II}Me]$^-$, **8a**, is more nucleophilic than [(L2)Pt^{II}Me]$^-$, **9a**. As mentioned above, the dispersion correction to the DFT-calculated activation energies in step *f* may be somewhat overestimated but the trend in calculated $\Delta G_{298}^{\#}$ matches the one observed in the experiment. Considering the relative reactivity of **8a** and **9a** in step *f*, we speculate that the lower nucleophilicity of [(L)Pt^{II}Me]$^-$ is responsible for a slower Pt^{IV}-to-Pt^{II} methyl transfer and slower formation of (*L*)Pt^{IV}Me$_2$ when ligand L2 is employed, as follows.

In the reaction of [(L2)Pt^{II}Me]$^-$ with O_2, the formation of the derived methylplatinum(IV) complex (L2)Pt^{IV}Me(OH), **11d**, occurs at a rate, which is somewhat higher than the rate of a subsequent Pt^{IV}-to-Pt^{II} methyl transfer, leading to the formation of (L2)Pt^{IV}Me$_2$, **13**, so that both **11d** (major) and **13** (minor) are observed in the reaction mixtures.

At the same time, in the oxidation of [(L1)Pt^{II}Me]$^-$ with O_2, all produced methylplatinum(IV) complex (L1)Pt^{IV}Me(OH), **10d**, is intercepted by a stronger nucleophile [(L1)Pt^{II}Me]$^-$ to form (L1)Pt^{IV}Me$_2$, **12**. As a result, **10d** is not observed in the reaction mixtures.

Finally, based on the reaction stoichiometry (Scheme 8, *b*), oxidation of **9** with O_2 in methanol produces methoxide anions, along with complex **11d**. We speculate that the rate of methyl group transfer from **11d** to methoxide, which is much less nucleophilic than **9a**, is slow so that **11d** can persist in the reaction mixtures.

Given a low stability and low yields of methylplatinum(IV) species observed in the reaction in MeOH solutions, as well as a very limited information about reactions leading to **11c** in aged reaction mixtures, the mechanism of the formation of **11c** currently remains purely speculative. As a working hypothesis, we assume that isomerization of **11d** to a slightly less stable **11c** was driven by much poorer solubility of the latter in MeOH and involved moderately unstable anionic adducts of **11d** and MeO$^-$ anion (Scheme S2; complexes **S1** and **S2**).

2.4.5. Aerobic Oxidation of K[(L2)Pt^{II}Me], 9, in Acetone-TFE Mixtures. Assuming that the nature of the solvent and the acidity of the reaction mixture used for oxidation of K[(L)Pt^{II}Me] may be an important factor affecting the reaction yield, selectivity, and the product stability, we attempted aerobic oxidation of K[(L2)Pt^{II}Me], **9**, in acetone. Given the need of a proton donor for aerobic oxidation of **9a** (Scheme 10), a mixture of acetone with 15 vol % of a protic co-solvent, TFE, was used in our next experiment. The protonolysis of **9** was minimal in this mixture, ∼5% overall, whereas the use of a noticeably larger than 15 vol % fraction of TFE led to a more pronounced decomposition of **9** and an increased formation of methane.

Stirring a suspension of **9** in the TFE-acetone mixture under an O_2 atmosphere for 12 h resulted in the complete consumption of **9** and the formation of two methylplatinum complexes, a dimethylplatinum(IV) complex (L2)Pt^{IV}Me$_2$, **13**, in 17% NMR yield, and a new monomethylplatinum(IV) complex in 61% NMR yield. The latter product was only stable in solution and decomposed upon attempted isolation. Its ^{1}H NMR spectrum exhibited a methyl ligand signal at 1.28 ppm with a coupling constant $^2J_{195PtH}$ of 71 Hz, suggesting the presence of a pyridyl fragment trans to the methyl. The selective difference NOE experiments involving acetone-d_6 solutions of the monomethylplatinum(IV) complex showed that a mutual arrangements in space of the methyl ligand, the terminal pyridine fragment of the pincer ligand L2, and its phenylene fragment are those expected for **11a** or its derivatives where the sulfonate group is displaced with an exogenous ligand (Figure S21).[29] The ESI mass spectra of the reaction mixtures showed the presence of anionic species [(L2)Pt^{IV}Me(OH)(OCH$_2$CF$_3$)]$^-$ (negative mode) and an adduct (L2)Pt^{IV}Me(OH)·K$^+$ (positive mode). The latter may result from a gas phase fragmentation of the former anionic complex. Since **11a** is expected to be kinetically unstable and to undergo a facile isomerization (Scheme S1, *d* and *e*), we propose that the reaction product observed in acetone/TFE mixtures is either **22** or **23** (Scheme 10). Based on our DFT calculations, the reaction of **11a** and CF$_3$CH$_2$O$^-$ anion to form complex **22** is more exergonic (−15.7 kcal/mol) than for its isomer **23** (−10.8 kcal/mol). At the same time, **23** is expected to be the primary product resulting from dissociation of the weakly bound SO$_3^-$ group from a Pt^{IV} center followed by coordination of CF$_3$CH$_2$O$^-$ to the metal (compare with the formation of **15**). Hence, we assume that the product observed in TFE-acetone mixtures is an anionic adduct **23**.

Comparing the methylplatinum(IV) complexes resulting from oxidation of **9** in MeOH and in a TFE-acetone mixture, a neutral complex **11d** in MeOH (Scheme 8), and an anionic **23** in the TFE-acetone mixture (Scheme 10), our DFT analysis helps account for this difference. According to our calculations, a displacement of the SO$_3^-$ group with MeO$^-$ and a Pt^{IV} center in **11d** is strongly endergonic in MeOH solutions (see **S1** in Scheme S2).

2.5. Reductive Elimination Reactivity of Monomethylplatinum(IV) Complexes Supported by L1 and L2. Reductive elimination study in this work was first carried out on isolated and well-characterized complexes **11c** and **15**. As it was shown earlier,[17] C(sp^3)-X coupling reactions (X = O and S) of complexes (L1)Pt^{IV}Me(Y), **5**, (Scheme 3, *a*) supported by the pincer ligand L1 can be promoted using solutions of trifluoroacetic acid in aqueous DMSO at 80 °C. This reagent was used in this work as well.

2.5.1. Reductive Elimination from 11c and 15. Complex **11c** was combined with ∼10:1 (vol) mixture of DMSO-d_6 and

https://doi.org/10.1021/acs.organomet.2c00371
Organometallics 2022, 41, 2764−2783

Scheme 11. Reductive Elimination of 11c and a 2:1 Mixture of 11c and 15 in 0.58 M CF_3COOD in a ~ 10:1 (vol) Mixture of DMSO-d_6 and D_2O at 80 °C.

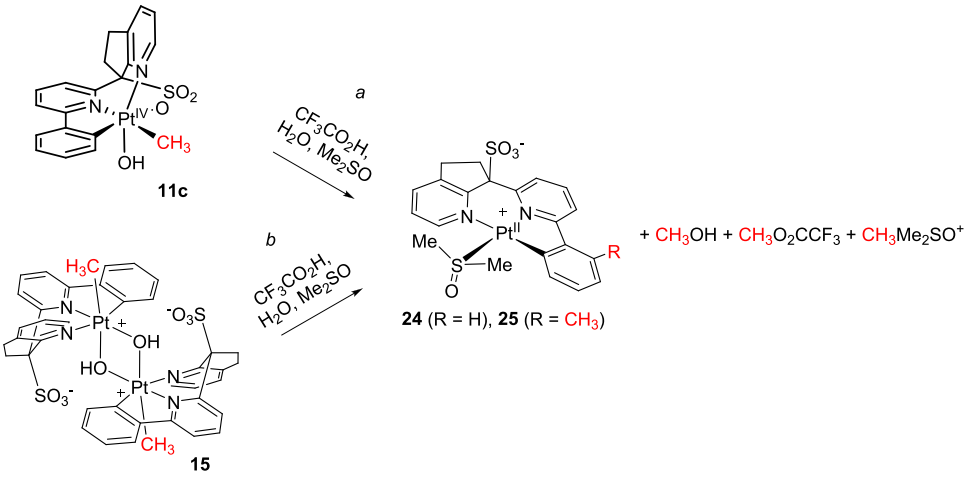

Scheme 12. Plausible Mechanism of Reductive Elimination of 11c and 15 in 0.58 M $DOOCCF_3$ in a ~10:1 (vol) Mixture of DMSO-d_6 and D_2O (Numbers in Blue Correspond to the Relative Reaction Gibbs Energies in kcal/mol (PBE-D3/LACVP/PBF(water)//PBE/LACVP** Level of Theory))**

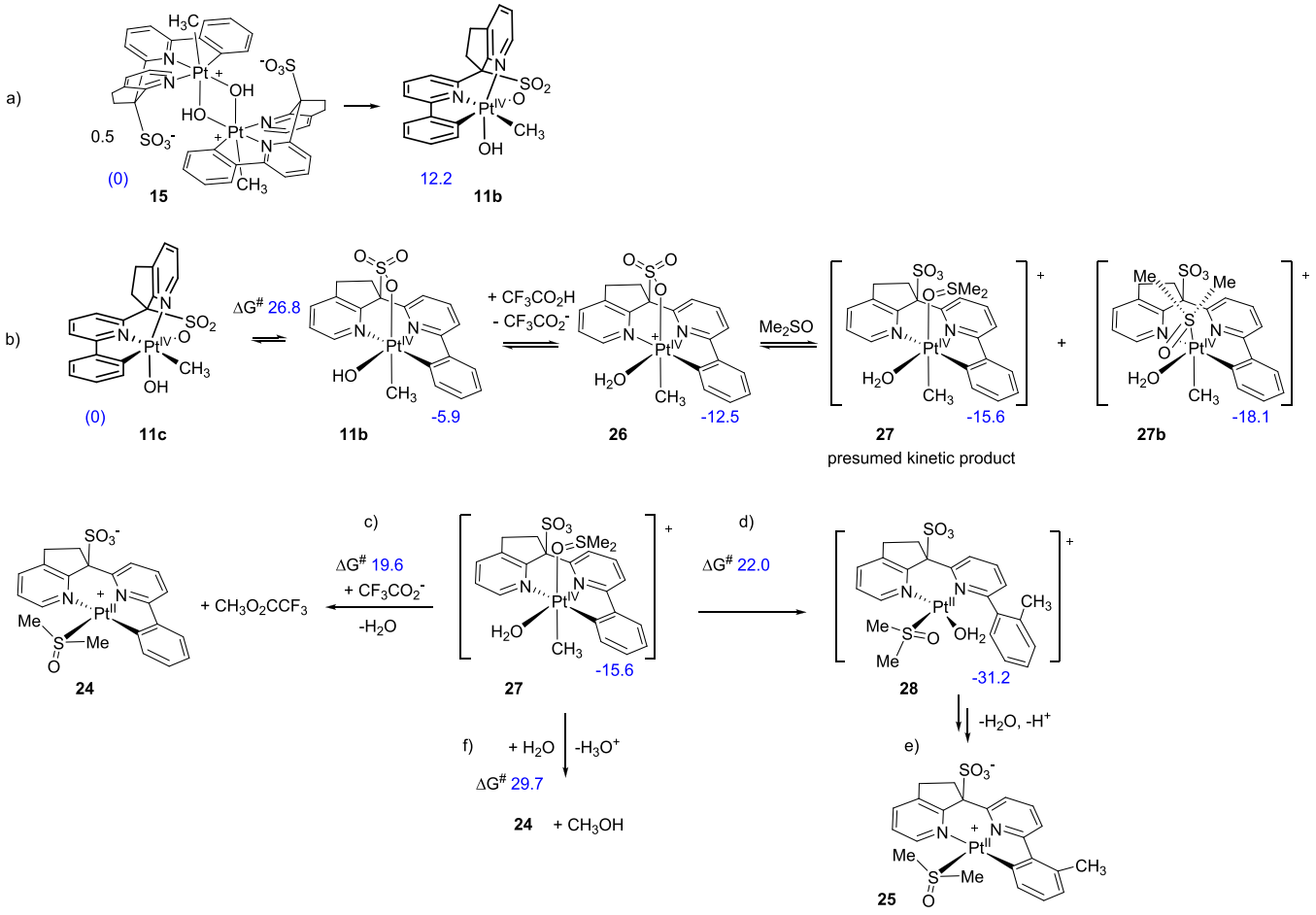

D_2O containing 0.58 M CF_3COOD. A ^1H NMR spectrum of the mixture exhibited a new set of signals that were shifted downfield, as compared to signals of **11c**, consistent with the formation of a protonated species $(L2)Pt^{IV}Me(OH_2)^+$, e.g., the $Pt^{IV}CH_3$ group signal shifted from 0.53 ppm for **11c** to 1.31 ppm for the presumed $(L2)Pt^{IV}Me(OH_2)^+$. Upon heating the mixture for 30 min at 80 °C, all solids dissolved and the $Pt^{IV}CH_3$ complex was fully consumed. The reaction products were identified by ^1H NMR (NMR yield and chemical shift for MeX derivatives are given in parentheses) as MeOH (80%; 3.17 ppm), CH_3OOCCF_3 (13%; 3.98 ppm),[17] $O{=}SMe_3^+$ (4%; 3.83 ppm),[17] $(L2)Pt^{II}$(DMSO), **24**, and $(L2^{Me})$-Pt^{II}(DMSO), **25**, (3%) (Scheme 11, *a*). Complex **24** was isolated and characterized by ^1H and ^{13}C NMR spectroscopy

https://doi.org/10.1021/acs.organomet.2c00371
Organometallics 2022, 41, 2764−2783

Scheme 13. Reductive Elimination of 11d in 0.22 M CF_3CO_2H or HBF_4 in 50% (vol) Aqueous MeOH; 11d was Used without Isolation

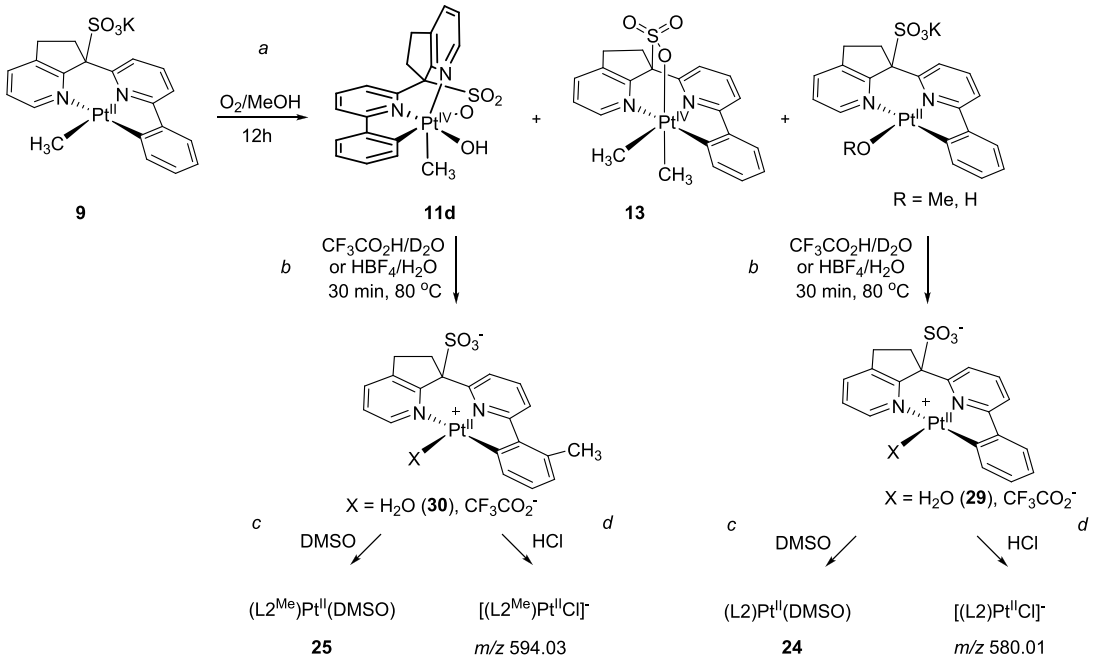

(Figures S17 and S18). The structure of the C−C coupled product **25** was proposed based on results of its ^{1}H NMR and ESI-MS characterization (see Section 2.5.2). A ^{1}H NMR spectrum of complex **25** in DMSO-d_6 exhibited a set of multiplets in the aromatic region including the most downfield signal of an *ortho*-pyridyl hydrogen atom at 8.77 ppm (dd, $^3J_{HH}$ = 5.4 Hz, J_{HH} = 0.8 Hz) integrating as 1H and a methyl group signal at 2.65 ppm integrating as 3H.

Since we were not able to separate **11c** from co-crystallized **15**, reductive elimination reactivity of **15** was probed using a 2:1 (mol) mixture of these compounds (Scheme 11, *a* and *b*). Upon heating the mixture of **11c** and **15** with 0.58 M CF_3COOD in DMSO-d_6/D_2O for 30 min at 80 °C, the Pt^{IV} complexes were consumed and a clear solution was produced. The solution contained, according to ^{1}H NMR (NMR yield is in parentheses), MeOH (88%), CH_3OOCCF_3 (4%), and O═SMe_3^+ (3%) as well as (L2)Pt^{II}(DMSO), **24**, and ($L2^{Me}$)-Pt^{II}(DMSO), **25** (5%).

Hence, based on the product distribution, there is no significant difference in the ability of **11c** and **15** to form the C(sp^3)-O coupled products, MeOH and MeO_2CCF_3. The latter two formed in a combined yield of ∼92% when using either pure **11c** or a 1:2 mixture of **15** and **11c**. Slightly different ratios of MeOH and MeO_2CCF_3 may be due to a slightly different extent of hydrolysis of the primary reaction product, MeO_2CCF_3, to form MeOH. The formation of ∼4% of O═SMe_3^+ is due to a non-negligible nucleophilicity of DMSO that served as a co-solvent. Finally, a C(sp^2)-C(sp^3) coupled product ($L2^{Me}$)Pt^{II}(OH_2), **25**, formed, on average, in ∼4% yield.

A plausible mechanism of the reactions above is given in Scheme 12. The isomerization of complex **11c** to **11b** is exergonic but is very slow at 25 °C (Scheme 12, *b*). This transformation is expected to be much faster at 80 °C used in our C(sp^3)-X elimination experiments. The protonation of **11b** with CF_3CO_2H is also weakly exergonic. Dissociation of the sulfonate group from a Pt^{IV} center and coordination of a DMSO molecule can produce exergonically two highly electrophilic isomeric adducts, both featuring a formal +2 charge on the metal center, a κ-*O*-DMSO adduct **27**, and a κ-*S*-DMSO adduct **27b**, which is 2.5 kcal/mol more stable. We presume that **27** is the kinetically preferred product (*vide infra*). The overall transformation of **11c** to **27** is characterized by the Gibbs energy change of −15.6 kcal/mol. The same species **27** can result from a dinuclear complex **15** (Scheme 12, *a*) also exergonically overall in reaction sequences *a* and *b*.

The κ-*O*-DMSO complex **27** undergoes a noticeably faster C(sp^3)-O and C(sp^3)-C(sp^2) reductive elimination than **27b** with 0.5−2.4 kcal/mol lower Gibbs activation energies, respectively (Scheme S3). We hypothesize that a lower steric demand of a κ-*O*-DMSO ligand in **27**, as compared to a κ-*S*-DMSO ligand in **27b**, can make **27** a kinetically preferred product in the series of transformations shown in Scheme 12, *a* and *b*. Accordingly, we presume that most of the products of C(sp^3)-X reductive elimination of **15** and **11c** (Scheme 12) are derived directly from **27**. Complex **27** is calculated to react with the $CF_3CO_2^-$ anion with a relatively low activation barrier of 19.6 kcal/mol to form $CH_3O_2CCF_3$ and complex **24** (Scheme 12, *c*). A slightly higher activation barrier, 22.0 kcal/mol, is required to achieve a C(sp^3)-C(sp^2) coupling to form an intermediate **28** (Scheme 12, *d*), which is expected to undergo cycloplatination and react in DMSO to form **25** (Scheme 12, *e*). Notably, a nucleophilic attack by H_2O molecule at **27** is characterized by a much higher Gibbs activation energy, 29.7 kcal/mol (Scheme 12, *f*). Hence, $CH_3O_2CCF_3$ is predicted to be the primary C(sp^3)-O coupled product that is then hydrolyzed by a water co-solvent to form MeOH. Overall, based on our DFT calculations, a 30:1 ratio of C(sp^3)-O and C(sp^2)-C(sp^3) coupled products is expected at 80 °C, close to the observed ratio of 92:4 = 23:1. The DFT-predicted ratio of C(sp^3)-O and C(sp^2)-C(sp^3) coupled products resulting directly from **27b** is 8000:1 (Scheme S3), a much poorer match to the experiment. Altogether, these results support our hypothesis that **27** and not **27b** is mostly

https://doi.org/10.1021/acs.organomet.2c00371
Organometallics 2022, 41, 2764−2783

Scheme 14. DFT-Calculated Gibbs Activation Energies for C(sp^2)-C(sp^3) over C(sp^3)-O Reductive Elimination of 11d in Acidic Aqueous Solutions (Numbers in Blue Correspond to the Relative Reaction Gibbs Energies in kcal/mol (PBE-D3/LACVP/PBF(H_2O)//PBE/LACVP** Level of Theory))**

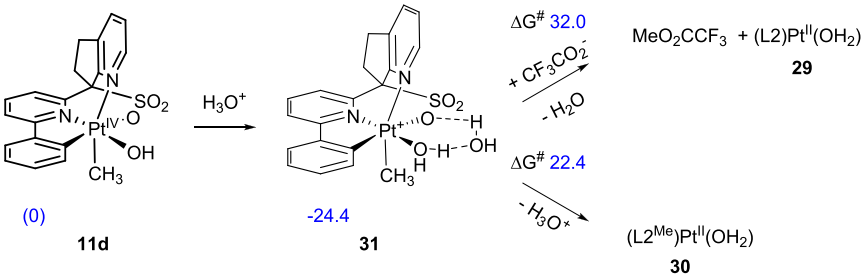

Scheme 15. Reductive Elimination of 23 in 0.22 M CF_3CO_2H in 50% (vol) Aqueous Acetone; 23 was Used without Isolation

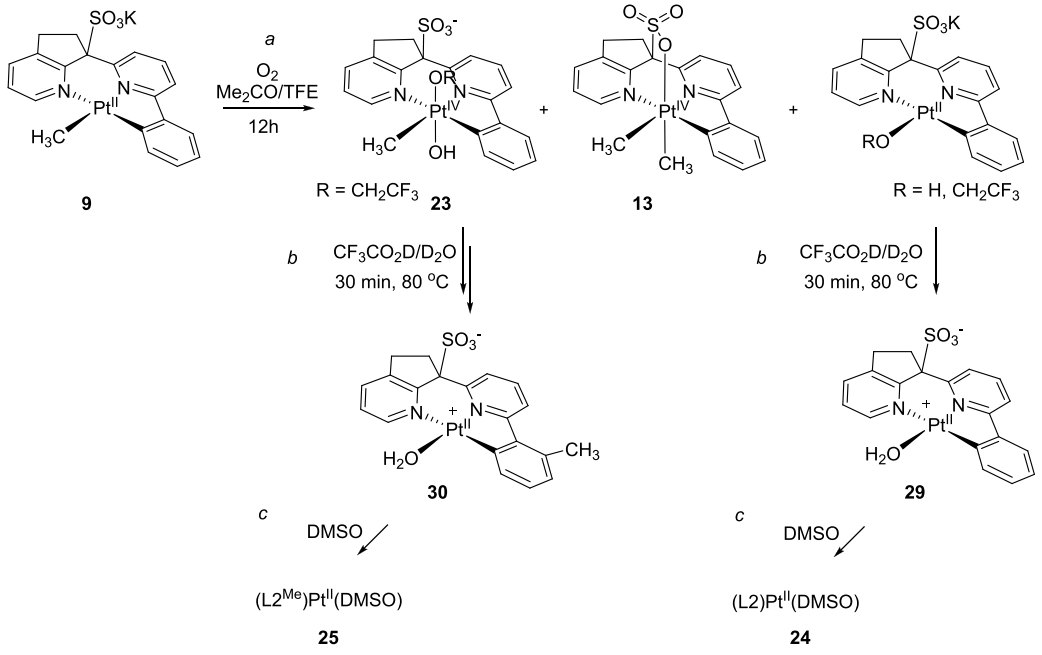

responsible for the C(sp^3)-X reductive elimination reactivity of **15** and **11c** in DMSO/H_2O/CF_3CO_2H solutions.

Finally, it is worth noting that the cationic aqua complex **26** was shown computationally to be much less reactive in both C(sp^3)-O_2CCF_3 and C(sp^2)-C(sp^3) coupling reactions with the activation barriers exceeding 30, 32.3, and 34.6 kcal/mol, respectively (Scheme S4).[29]

Overall, the factors that appear to be the most critical ones favoring the C(sp^3)-O coupling of **11c**, **11b**, and **15** are (i) the ability of a (L)Pt^{IV}Me(OH) complex to readily attain a configuration featuring a *trans-* arrangement of the methyl ligand being eliminated and the sulfonate (a good leaving group), (ii) the presence of DMSO in the reaction mixtures leading to the formation of a highly electrophilic DMSO adduct such as **27** with a formal +2 charge on a Pt^{IV} center, and (iii) the presence of a $CF_3CO_2^-$ anion, which is a more potent nucleophile than water or DMSO.

*2.5.2. Reductive Elimination of **11d**.* Since two products of oxidation of **9** with O_2, **11a** (its anionic adduct **23**) and **11d**, were unstable and observed only in solutions, we decided to probe their reductive elimination reactivity *in situ* using reaction mixtures resulting from oxidation of **9** with O_2 in acetone-d_6/TFE (Scheme 10) or MeOH-d_4 (Scheme 8, *b*), respectively.

A solution of **11d** in MeOH-d_4 was prepared by stirring a suspension of complex **9** in this solvent under 1 atm pressure of O_2 (Scheme 13, *a*). After 12 h, the solution contained predominantly **11d** and a mixture of K[(L2)Pt^{II}(OR)] (R = H and Me), whereas most part of the less soluble minor byproduct (L2)$Pt^{IV}Me_2$, **13**, precipitated and was separated by filtration. The liquid was combined with an equal volume of 0.44 M solution of CF_3CO_2D in D_2O and heated at 80 °C (Scheme 13, *b*). After 30 min, complex **11d** was fully consumed. Neither CH_3OH nor $CH_3O_2CCF_3$ was produced. Two new singlets at 2.52 and 2.59 ppm appeared in a ^{1}H NMR spectrum. Based on the tests mentioned below, the signals were assigned to K[(L2^{Me})Pt^{II}(O_2CCF_3)] or [(L2^{Me})-Pt^{II}(MeOH)] and [(L2^{Me})Pt^{II}(OH_2)], **30**, respectively. Addition of D_2O to the mixture increased the intensity of the 2.59 ppm signal at the expense of the signal at 2.52 ppm, supporting the assignment of the former signal to [(L2^{Me})-Pt^{II}(OH_2)], **30**. Taken together, the signals accounted for ~100% of the methyl ligand balance. In addition to K[(L2^{Me})Pt^{II}(O_2CCF_3)] and [(L2^{Me})Pt^{II}(OH_2)], **30**, two more pincer ligand-containing species were observed in the reaction solution by ^{1}H NMR spectroscopy. As it follows from the following observations, we presume that these species are [(L2)Pt^{II}(OH_2)], **29**, and K[(L2)Pt^{II}(O_2CCF_3)] or [(L2)-

https://doi.org/10.1021/acs.organomet.2c00371
Organometallics 2022, 41, 2764−2783

Scheme 16. Transformation of 23 to 11a and 11d in Acidic Aqueous Solutions (Numbers in Blue Correspond to the Relative Reaction Gibbs Energies in kcal/mol (PBE-D3/LACVP/PBF(H_2O)//PBE/LACVP** Level of Theory))**

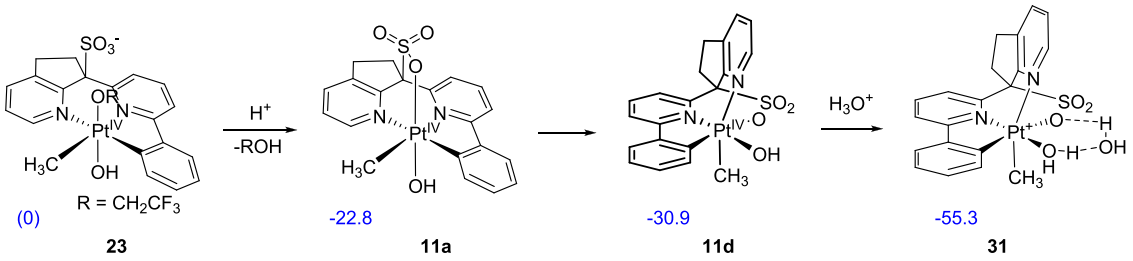

Pt^{II}(MeOH)]. Next, all volatiles were removed from the reaction solution under vacuum and the resulting solid was dissolved in DMSO-d_6 (Scheme 13, *c*). A ^{1}H NMR spectrum showed the presence of only two pincer ligand-containing species, (L2)Pt^{II}(DMSO), **24**, and ($L2^{Me}$)Pt^{II}(DMSO), **25** (Figure S25).

To characterize the reaction products by means of ESI-MS, oxidation of **9** was repeated by employing CH_3OH as a solvent. A subsequent reductive elimination reaction was carried out using aqueous HBF_4. The resulting reaction solution was combined with aqueous HCl to form a mixture of anions, $[(L2)Pt^{II}Cl]^-$ and $[(L2^{Me})Pt^{II}Cl]^-$, (Scheme 13, *d*) that were detected by means of ESI-MS (negative mode).

The observed preference of a C(sp^2)-C(sp^3) over C(sp^3)-O reductive elimination of **11d** was supported using DFT calculations. For simplicity, purely aqueous solutions were considered (Scheme 14). An adduct **31** of a protonated complex **11d** and one water molecule that hydrogen-bridges the aqua ligand and a sulfonate oxygen atom was found to be the most reactive in the C(sp^2)-C(sp^3) reductive elimination. The formation of **31** was predicted to be exergonic. The Gibbs activation energy of the C(sp^2)-C(sp^3) coupling of **31** is 22.4 kcal/mol, whereas the C(sp^3)-O coupling of **31** and the $CF_3CO_2^-$ anion has a much higher Gibbs activation energy of 32.0 kcal/mol. Similarly, high Gibbs activation energies for C(sp^3)-O coupling were found for a number of other **11d**-derived species.

*2.5.3. Reductive Elimination of **23**.* A solution of a trifluoroethoxide adduct of **11a**, **23**, was prepared by stirring a suspension of **9** in a 15 (vol) % TFE-acetone mixture under an O_2 atmosphere for 12 h, and a solid byproduct **13** was separated by filtration (Scheme 15, *a*). The resulting liquid was combined with an equal volume of 0.44 M CF_3CO_2D in D_2O, and the mixture was exposed to 80 °C for 30 min (Scheme 15, *b*). ^{1}H NMR spectroscopy revealed the complete consumption of **23** and the appearance of one new singlet at 2.52 ppm, which was associated with a C−C coupled reaction product ($L2^{Me}$)$Pt^{II}(OH_2)$, **30**, formed in 70% NMR yield. Upon removal of volatile components, the residue was dissolved in DMSO-d_6 and was shown by ^{1}H NMR spectroscopy to contain a mixture of **24** and **25** (Scheme 15, *c*; Figure S26).

Assuming that **23** can be readily converted to **11a** in acidic aqueous solutions (Scheme 16) and given a facile interconversion of **11a** and **11d** (Scheme 7, *b*), it is not surprising that **23** (via **11a**) undergoes a C(sp^2)-C(sp^3) reductive elimination, similar to the behavior of **11d** (Scheme 14). A computational (DFT) analysis (Scheme 16) shows a proposed sequence of exergonic reactions leading from **23** to **31** in acidic aqueous solutions. The latter complex can selectively eliminate a C(sp^2)-C(sp^3) coupled product (Scheme 14).

Overall, the key factors that appear to favor the C(sp^3)-C coupling of **11a** and **11d** are (i) an existing or a readily attainable arrangement of the sulfonate group *trans* to the pincer ligand carbon atom (CNO-coordination of L) and (ii) an existing or a readily attainable axial arrangement of the methyl ligand.

*2.5.4. Reductive Elimination of **10c**.* Complex (L1)Pt^{IV}Me(OH), **10c**, prepared by oxidation of **8** with H_2O_2 in MeOH solutions was used in C(sp^3)-X reductive elimination experiments. This compound was poorly soluble in DMSO-d_6 even at 85 °C but in the presence of 0.40 M CF_3CO_2D at 85 °C, **10c** dissolved readily to produce a clear solution. According to ^{1}H NMR spectroscopy, **10c** was fully consumed in 2 h and the resulting solution (NMR yield is in parentheses) contained MeOH (4%) and MeO_2CCF_3 (87%), along with 9% Me_3SO^+; no C(sp^3)-C(sp^2) coupled products were detected (Scheme 17, *a*). Hence, similar to **11c**, **10c** produces predominantly

Scheme 17. Reductive Elimination of 10c in 0.40 M CF_3COOH Solutions of (a) DMSO-d_6 and (b) D_2O at 85 °C

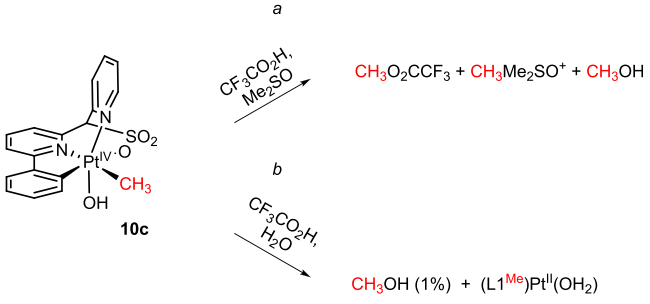

C(sp^3)-O coupled products, MeOH and MeO_2CCF_3, but, due to water being present in a sample of DMSO-d_6 as a small impurity only, the major reaction product was the ester, MeO_2CCF_3. Remarkably, when **10c** was heated with 0.40 M CF_3CO_2H solution in D_2O at 85 °C for 2 h, the reaction resulted only in 1% yield of MeOH with the major product being a of C−C coupled compound ($L1^{Me}$)$Pt^{II}(OH_2)$, exhibiting a singlet at 2.63 ppm (Scheme 17, *b*). The latter observation points, once again, to the importance of using DMSO as a co-solvent helping achieve an efficient C(sp^3)-O coupling.

3. CONCLUSIONS

In this work, two tetradentate rigid sulfonated CNN-pincer ligands, L1 and L2, that impose a distorted octahedral geometry on a Pt^{IV} center were used to affect the reactivity of derived platinum complexes in aerobic Pt^{II}-Me bond functionalization: (i) a Pt^{II}-to-Pt^{IV} oxidation of K[(L)Pt^{II}Me] (L = L1 and L2) with O_2 in protic media and (ii) C(sp^3)-X

https://doi.org/10.1021/acs.organomet.2c00371
Organometallics 2022, 41, 2764−2783

reductive elimination (X = O and C) of the resulting (L)$Pt^{IV}Me(OH)$ complexes in an acidic environment. Although a clean/high yielding aerobic Pt^{II}-Me bond functionalization was accomplished earlier using di(pyrid-2-yl)methanesulfonate (dpms) family ligands,[18] a recently demonstrated arene ArH $C(sp^2)$-H bond activation with $(L1)Pt^{II}(H_2O)$ and oxidation with O_2 of the resulting "$(L1)Pt^{II}Ar$" transient to form $(L1)Pt^{IV}Ar(OH)$[11] hinted on a potential realization of a catalytic aerobic $C(sp^3)$-H functionalization when alkane derivatives are employed. In this work, we found that the rigidity of L1 and L2 and a poor match of their geometry to a Pt^{IV} octahedral coordination result, in general, in a diminished configurational stability and enhanced reactivity of the supported (L)$Pt^{IV}Me(OH)$ complexes. Since ligands L1 and L2 do not provide the same level of stabilization of a Pt^{IV} center as dpms does, the new ligands (i) enabled a slower (L1 > L2) and a less selective oxidation with O_2 of the derived $K[(L)Pt^{II}Me]$ complexes and (ii) facilitated a facile interconversion of the resulting diastereomeric complexes (L)$Pt^{IV}Me(OH)$, which, along with (i), led to the exclusive (L1) or noticeable (L2) formation of Pt^{IV}-to-Pt^{II} methyl transfer products, (L)$Pt^{IV}Me_2$. The latter reaction along with a competing protonolysis of $K[(L2)Pt^{II}Me]$ was the reason for a lower, 30% (MeOH solutions)−60% (acetone/TFE mixtures) selectivity in (L2)-$Pt^{IV}Me(OH)$ in the reactions of $K[(L2)Pt^{II}Me]$ with O_2. Remarkably, an enhanced rigidity of ligand L2 that resulted from the introduction of a fused cyclopentane ring allowed to suppress the bimolecular[26] Pt^{IV}-to-Pt^{II} methyl transfer and to diminish the formation of (L)$Pt^{IV}Me_2$. This change in reactivity was proposed to be due to the decreased nucleophilicity of the $[(L2)Pt^{II}Me]^-$ anion, as compared to that of $[(L1)Pt^{II}Me]^-$. Notably, in hypothetical catalytic systems for methane functionalization, the concentration of $[(L)Pt^{II}Me]^-$ species is expected to be very low so that the formation of (L)$Pt^{IV}Me_2$ may become unobservable. Overall, all four diastereomeric complexes (L2)$Pt^{IV}Me(OH)$ or their anionic derivatives were isolated or observed in reactions of $K[(L2)Pt^{II}Me]$ with O_2 and/or H_2O_2. The formation of specific diastereomers was explained in terms of the predominance (O_2, slow reactions) or virtually equal probability (H_2O_2, diffusion-controlled reactions) of the attack of the oxidant, O_2 or H_2O_2, at a Pt^{II} center present in the $[(^{CNN}L2)Pt^{II}Me]^-$ anion, occurring from either the top or the bottom of the metal coordination unit. Our study of the $C(sp^3)$-X reductive elimination reactivity of (L2)$Pt^{IV}Me(OH)$ in acidic solutions at 80 °C showed that two most reactive diastereoisomers produced exclusively $C(sp^2)$-$C(sp^3)$ coupled products. Remarkably, the remaining two kinetically more robust diastereomeric complexes (L2)$Pt^{IV}Me(OH)$ reacted with CF_3CO_2H in aqueous DMSO to form, in a high combined yield, the $C(sp^3)$-O coupled products, MeOH and MeO_2CCF_3, with only a trace (≤4%) amount of $C(sp^2)$-$C(sp^3)$ coupled derivatives. Our computational (DFT) analysis suggested that the key factors that favor the $C(sp^3)$-O over the $C(sp^2)$-$C(sp^3)$ coupling of (L)$Pt^{IV}Me(OH)$ in acidic solutions are (i) a readily attainable configuration of (L)$Pt^{IV}Me(OH)$ with a *trans* arrangement of the methyl ligand and the sulfonate group, (ii) the use of $CF_3CO_2^-$ as a more potent nucleophile than water, and (iii) the use of DMSO as a specific additive that allows for the formation of highly electrophilic intermediates that have a dramatically lower activation barrier of the $C(sp^3)$-O coupling. The formation of $C(sp^2)$-$C(sp^3)$ coupled products is one of the key problems that remains to be solved on the way to the development of catalytic aerobic methane functionalization utilizing sulfonated CNN-pincer ligands−Pt(II) platforms. We expect that some appropriate modifications of our pincer ligands may allow one to solve this problem. Overall, the lessons learned from this study can guide the future rational design of ligands and metal complexes for aerobic organometallic chemistry.

4. EXPERIMENTAL SECTION

4.1. General Considerations. Reactions requiring exclusion of air and/or moisture were carried out under an argon atmosphere. All reagents for which synthesis is not reported were purchased from Sigma-Aldrich, Oakwood Chemical, Matrix Scientific, or Pressure Chemical and used without purification unless otherwise noted. Silica gel SEPIX 56040 (63 μm) was purchased from ZEOCHEM and used for all column chromatography purifications. The pre-ligand H_2L1,[14] $Pt_2Me_4(SMe_2)_2$,[34] $K[(L1)Pt^{II}Me]$, **8**,[17] and $[(L1)Pt^{IV}Me_2]$, **13**,[17] were synthesized according to the literature. TFE from Sigma-Aldrich or Oakwood Chemical was dried over calcium hydride, purified by vacuum transfer, and stored in an argon-filled glovebox. THF and Et_2O solvents were dried over and distilled from sodium/benzophenone adduct and stored over molecular sieves under argon. Deuterium-labeled solvents MeOD-d_4, $CDCl_3$, and DMSO-d_6 were purchased from Cambridge Isotope Laboratories and CF_3CH_2OD (TFE-d_1) was purchased from Sigma-Aldrich. ^{1}H NMR (400, 500, and 600 MHz) and ^{13}C NMR (100, 125, and 150 MHz) spectra were recorded on a Bruker AVANCE 400 MHz, a Bruker DRX-500 MHz, or a Bruker AVIII-600 MHz spectrometer. Chemical shifts are reported in parts per million (ppm) (δ) and referenced to residual solvent peaks. Multiplicities are reported as follows: br (broad signal), s (singlet), d (doublet), t (triplet), q (quartet), quin (quintet), sex (sextet), m (multiplet), dd (doublet of doublets), dt (doublet of triplets), and qd (quartet of doublets). Coupling constants (J) are reported in Hz. High-resolution mass spectrometry (HRMS) experiments were performed using a JEOL AccuTOF-CS instrument.

4.2. Synthesis of Pre-ligand H_2L2. *4.2.1. 2-Fluoro-6-phenylpyridine, S1.* 21.98 g (0.125 mol) of 2-bromo-6-fluoropyridine, 22.8 g (0.187 mol) of phenylboronic acid, 57.54 g (0.25 mol) of $K_3PO_4\cdot H_2O$, 500 mL of $HO(CH_2)_2OH$, and 0.2806 g (1.25 mmol) of $Pd(OAc)_2$ were added to a 1 L round-bottom flask. A stir bar was added, and the round-bottom flask was put in a 55 °C oil bath. After a 3 h of stirring, 1250 mL of brine was mixed with the reaction mixture. Et_2O was then used to extract the product (1250 mL × 3). Afterward, $MgSO_4$ was used to dry the combined organic phase and filtered off followed by solvent removal. Lastly, silica gel column chromatography was used to obtain a pure product. Eluent: hexane. The product was obtained as a colorless oil with a yield of 15 g (70%). ^{1}H NMR (400 MHz, 22 °C, $CDCl_3$), δ: 8.01 (vd, $^3J_{HH}$ = 8 Hz, 2H, Ph, *o*-H), 7.83 (m, 1H, py, C3-H), 7.62 (dd, $^3J_{HH}$ = 8 Hz, $^4J_{HH}$ = 4 Hz, 1H, py, C5-H), 7.50−7.43 (m, 3H, Ph, *m*-, *p*-H), 6.86 (dd, 1H, $^3J_{HH}$ = 8 Hz, $^4J_{HH}$ = 4 Hz, py, C3-H) (Figure S1).

4.2.2. 7-(6-Phenylpyrid-2-yl)-6,7-dihydro-5H-cyclopenta[b]-pyridine, S2. In a glovebox, 20.6 g (0.173 mol) of 6,7-dihydro-5*H*-cyclopenta[*b*]pyridine, 125 mL of dried THF, and a stir bar were added into a dried 250 mL Schlenk tube. Under an Ar atmosphere and −78 °C, *n*-BuLi solution (11 M) was added dropwise into the Schlenk tube. The Schlenk tube was then capped and its contents were stirred for 30 min before being warmed to 0 °C for an additional 30 min stir. The Schlenk tube was then cooled back to −78 °C and into it were added 15 g (0.087 mol) of **S1**. After that, the Schlenk tube was capped, warmed to r.t. and left to stir for 24 h. To work up this reaction, water was added to the Schlenk tube. The reaction mixture was then rotovapped down to near-dryness and Et_2O (100 mL × 3) and water (100 mL) were used to extract the product from the reaction mixture. The organic phases were combined, dried by $MgSO_4$, separated from solid by filtration, and rotovapped to dryness. Silica gel column chromatography was used to isolate **S2** and excess 6,7-dihydro-5*H*-cyclopenta[*b*]pyridine. Eluent: hexane:EA:TEA =

https://doi.org/10.1021/acs.organomet.2c00371
Organometallics 2022, 41, 2764−2783

5:1:0.01. **S2** was obtained as yellow oil with a yield of 14.2 g (60%). ^{1}H NMR (400 MHz, 22 °C, $CDCl_3$), δ: 8.38 (d, $^3J_{HH}$ = 4.9 Hz, 1H, pyridyl-*ortho* H), 8.02−7.96 (m, 2H, ArH), 7.68−7.61 (m, 1H, ArH), 7.57−7.49 (m, 2H, ArH), 7.46−7.38 (m, 2H, ArH), 7.38−7.32 (m, 1H, ArH), 7.20 (d, $^3J_{HH}$ = 7.7 Hz, 1H, ArH), 7.05−6.98 (m, 1H, ArH), 4.66 (t, $^3J_{HH}$ = 7.6 Hz, 1H, CH), 3.28−3.16 (m, 1H, CH_2CH_2), 3.03−2.91 (m, 1H, CH_2CH_2), 2.64 (d, $^3J_{HH}$ = 7.5 Hz, 2H, CH_2CH_2) (Figure S2). ^{13}C NMR (600 MHz, 22 °C, $CDCl_3$), δ: 166.0, 162.6, 156.5, 147.6, 139.5, 137.5, 137.0, 132.4, 128.5, 128.4 (2C), 126.8 (2C), 121.4, 121.0, 118.0, 53.8, 31.1, 29.7 (Figure S3).

4.2.3. H_2L2. In a glovebox, 4.2 g (15.4 mmol) of **S2**, 30 mL of THF, 2.47 g (92.5 mmol) of NaH (90% purity), and a stir bar were added to a dried 50 mL Schlenk tube. The Schlenk tube was capped and submitted to heating and stirring at 50 °C for 24 h. During the heating, the Schlenk tube was vented frequently. After the heating time was reached, the Schlenk tube was cooled to r.t., and 2.45 g (15.4 mmol) of sulfur trioxide pyridine complex was added under Ar. Then, the reaction was stirred at 70 °C for 24 h. When the reaction was done, a large amount of solid formed. A small amount of ice-cold water was added to the Schlenk tube to quench the reaction. The resulting reaction suspension was extracted by Et_2O (50 mL × 3) to recover unreacted **S2**. The solid and the aqueous phase were put into a separate beaker with about 1 L of water and a stir bar added. After being stirred for 0.5 h, the mixture was passed through a Buchner funnel to remove any water-insoluble solid. The aqueous solution was then acidified by H_2SO_4 (aq) to pH = 1. With an additional 30 min stir, the precipitate formed, which was then collected by vacuum filtration. The product was a grayish brown solid. Yield: 2.4 g (44%). ^{1}H NMR (400 MHz, 22 °C, DMSO-d_6), δ: 8.76 (d, $^3J_{HH}$ = 5.6 Hz, 1H, pyridyl-*ortho* H), 8.49 (d, $^3J_{HH}$ = 7.6 Hz, 1H, ArH), 7.98 (t, $^3J_{HH}$ = 7.9 Hz, 1H, ArH), 7.96−7.87 (m, 5H, ArH), 7.47−7.38 (m, 3H, ArH), 3.32−3.22 (m, 2H, CH_2CH_2), 3.16−3.06 (m, 1H, CH_2CH_2), 2.73−2.64 (m, 1H, CH_2CH_2) (Figure S4). ^{13}C NMR (600 MHz, 22 °C, DMSO-d_6), δ: 158.3, 155.8, 153.7, 144.7, 142.0, 139.2, 138.2, 138.1, 129.1 (2C), 128.7 (2C), 126.8, 125.4, 122.2, 119.2, 76.6, 35.7, 28.6 (Figure S5). ESI-MS(−) in H_2O: $(HL2)^-$: 351.0800, calculated for $[C_{19}H_{15}N_2O_3S]^-$, 351.0809.

4.3. Synthesis of K[(L1)Pt^{II}Me], 8. Preparation of complex **8** was carried out as reported previously.[17] When **8** was dissolved in CD_3OD, the extent of its methanolysis was ∼19% after 10 h of reaction at 20 °C. A slow H/D exchange was observed in the methyl group of the complex with the extent of deuteration approaching 19% after the same period of time. X-ray quality crystals of **8** were obtained by layering a saturated MeOH-THF solution of **8** with an equal volume of Et2O.

4.4. Synthesis of K[(L2)Pt^{II}Me], 9. This method is analogous to the one used in the synthesis of **8**.[17] In a glovebox, the pre-ligand **H_2L2** (0.331 g, 0.94 mmol), KO*t*Bu (0.106 g, 0.94 mmol), and a stir bar were added to a vial. $Pt_2Me_4(SMe_2)_2$ (180 mg, 0.31 mmol) was placed in a separate vial in the glovebox. MeOH was added to two vials. The suspension of $Pt_2Me_4(SMe_2)_2$ was transferred to the other vial, and a total volume of 25 mL MeOH was used. The mixture was capped and stirred for 5 days. A yellow suspension formed, and the solution was filtered. The filter cake was collected, dried under vacuum at room temperature, and appeared as a yellow solid. Yield: 300 mg (0.50 mmol), 80%. The product is unstable under air. ^{1}H NMR (600 MHz, 22 °C, DMSO-d_6), δ: 8.70 (d, $^3J_{HH}$ = 5.5 Hz, 1H, pyridyl-*ortho* H), 7.97 (t, $^3J_{HH}$ = 7.9 Hz, 1H, ArH), 7.93 (d, $^3J_{HH}$ = 7.5 Hz, 1H, ArH), 7.90 (d, $^3J_{HH}$ = 7.8 Hz, 1H, ArH), 7.65 (d, $^3J_{HH}$ = 7.5 Hz, 1H, ArH), 7.60 (d, $^3J_{HH}$ = 7.5 Hz, 1H, ArH), 7.52 (d, $^3J_{HH}$ = 7.8 Hz, 1H, ArH), 7.37 (dd, $^3J_{HH}$ = 7.7 Hz, J_{HH} = 5.9 Hz, 1H, ArH), 7.04 (t, $^3J_{HH}$ = 7.2 Hz, 1H, ArH), 6.94 (t, $^3J_{HH}$ = 7.4 Hz, 1H, ArH), 3.45−3.34 (m, hidden in the water signal, CH_2CH_2), 2.99 (dd, J_{HH} = 9.8 Hz, J_{HH} = 14.5 Hz, 1H, CH_2CH_2), 2.68 (q, $^3J_{HH}$ = 11.8 Hz, 1H, CH_2CH_2), 1.00 (s, $^2J_{195PtH}$ = 78 Hz, 3H, $PtCH_3$) (Figure S6). ^{13}C NMR (150 MHz, 22 °C, DMSO-d_6), δ: 163.0, 157.7, 155.7, 148.1, 147.2, 145.7, 142.5, 136.2, 132.9, 132.6, 128.0, 123.9, 123.5, 123.5, 121.3, 116.6, 81.1, 37.1, 28.8, −8.4 (Figure S7). ESI-MS(−) in MeOH: $[(L2)PtMe]^-$: 560.0433, calculated for $[C_{20}H_{17}N_2O_3SPt]^-$, 560.0613.

4.5. Effect of Counterion Na$^+$. In a glovebox, **NaHL2** (56.2 mg, 0.15 mmol), prepared from NaH and **H_2L2** and a stir bar were added to a vial. Three milliliters of MeOH was added into the vial, and stirring was started. $Pt_2Me_4(SMe_2)_2$ (28.7 mg, 0.05 mmol) was added into the vial under stirring. The mixture was capped and stirred for 6 days. A green suspension formed, and the solution was filtered. The filter cake was collected and dried under vacuum at room temperature. The yield of Na[(L2)Pt^{II}Me] was 30 mg (51%).

4.6. Preparation of ^{n}Pr$_4$N[(C$_6$H$_4$-pcpps)Pt^{II}Me], 9*. This synthesis was carried out in a glovebox. Fifty milligrams of **9** was dissolved in acetone (∼1 mM, filter off excess solid) followed by ^{n}Pr$_4$NCl. The solution was evaporated under vacuum. DCM was then used to extract the solid residue. At last, the DCM solution (filtration was applied if there was any white solid in it) was evaporated under vacuum to yield 56 mg of yellow solid as the product. The yield was 79%, and the purity of the yellow solid was 88% based on NMR. No other ligand-containing species were observed in the spectrum, and the impurity was ^{n}Pr$_4$NCl. Crystals suitable for X-ray diffraction were obtained by dissolving the product in MeOH + Et_2O + heptane followed by slow evaporation in the glovebox at −4 °C. ^{1}H NMR (600 MHz, 22 °C, DMSO-d_6), δ: 8.70 (d, $^3J_{HH}$ = 5.7 Hz, 1H, pyridyl-*ortho* H), 7.97 (t, $^3J_{HH}$ = 7.9 Hz, 1H, ArH), 7.93 (dd, $^3J_{HH}$ = 7.9 Hz, $^3J_{HH}$ = 0.9 Hz, 1H, ArH), 7.90 (dd, $^3J_{HH}$ = 8.1 Hz, $^3J_{HH}$ = 1.0 Hz, 1H, ArH), 7.64 (dd, $^3J_{HH}$ = 8.1 Hz, $^3J_{HH}$ = 1.2 Hz, 1H, ArH), 7.60 (dd, $^3J_{HH}$ = 7.6 Hz, $^3J_{HH}$ = 1.0 Hz, 1H, ArH), 7.52 (dd, $^3J_{HH}$ = 8.0 Hz, $^3J_{HH}$ = 1.0 Hz, 1H, ArH), 7.37 (dd, $^3J_{HH}$ = 8.0 Hz, J_{HH} = 5.7 Hz, 1H, ArH), 7.04 (dt, $^3J_{HH}$ = 7.3 Hz, $^3J_{HH}$ = 1.2 Hz, 1H, ArH), 6.94 (dt, $^3J_{HH}$ = 7.4 Hz, $^3J_{HH}$ = 1.3 Hz, 1H, ArH), 3.45−3.33 (m, CH_2CH_2), 3.17−3.07 (m, 8H, $NCH_2CH_2CH_3$), 2.99 (dd, J_{HH} = 14.9 Hz, J_{HH} = 9.7 Hz, 1H, CH_2CH_2), 2.72−2.64 (m, 1H, CH_2CH_2), 1.66−1.55 (m, 8H, $NCH_2CH_2CH_3$), 1.00 (s, $^2J_{195PtH}$ = 80 Hz, 3H, $PtCH_3$), 0.89 (t, $^3J_{HH}$ = 7.3 Hz, 12H, $NCH_2CH_2CH_3$).

4.7. Preparation of (L1)Pt^{IV}Me$_2$, 12. Complex **12** was prepared as reported earlier.[17] X-ray quality crystals of **12** were obtained by slow evaporation of TFE solution of **12**.

4.8. Preparation of (L2)Pt^{IV}Me$_2$, 13. Twenty milligrams of (0.0334 mmol) **9** was dissolved in 40 mL of acetone in a round-bottom flask to make a yellow/green solution (any insoluble solid was filtered off). A stir bar was added, as well as 0.0415 mL (0.667 mmol) of CH_3I. With fast stirring, the solution became colorless within minutes. The solution was concentrated to produce **13** as a white precipitate. When there was about 1 mL of acetone left, filtration was done to collect the product. Yield: 14 mg (73%). Crystals suitable for X-ray diffraction were obtained when aerobic oxidation of **9** was carried out in MeOH. The products **13** and **13b** have different distributions in different solvents. In acetone-d_6 and CH_3CN-d_3, ratios of **13**:**13b** are 1:0.83 and 1:0.4, respectively. In TFE or HFIP, only **13** shows up. **13** undergoes degradation to produce a violet solution in HFIP if left for days. **13**, ^{1}H NMR (400 MHz, 22 °C, TFE), δ: 8.50 (d, $^3J_{HH}$ = 5.5 Hz, 1H, pyridyl-*ortho* H), 8.09−8.00 (m, 2H, ArH), 7.98 (d, $^3J_{HH}$ = 7.6 Hz, 1H, ArH), 7.82−7.73 (m, 2H, ArH), 7.56 (d, $^3J_{HH}$ = 7.5 Hz, 2H, ArH), 7.32−7.19 (m, 2H, ArH), 1.44 [s, $^2J_{HPt}$ = 62 Hz, 3H, Pt(equatorial-CH_3)], 1.14 [s, $^2J_{HPt}$ = 80 Hz, 3H, Pt(axial-CH_3)]. CH_2CH_2 moiety overlaps with a solvent signal. ^{1}H NMR (400 MHz, 22 °C, HFIP), δ: 8.54 (d, $^3J_{HH}$ = 5.5 Hz, 1H, pyridyl-*ortho* H), 8.15−7.99 (m, 3H, ArH), 7.86−7.78 (m, 2H, ArH), 7.71−7.54 (m, 2H, ArH), 7.34 (t, $^3J_{HH}$ = 7.2 Hz, 1H ArH), 7.29 (t, $^3J_{HH}$ = 7.3 Hz, 1H ArH), 3.61−3.48 (m, 1H, CH_2CH_2), 3.48−3.24 (m, 3H, CH_2CH_2), 1.52 [s, $^2J_{HPt}$ = 64 Hz, 3H, Pt(equatorial-CH_3)], 1.26 [s, $^2J_{HPt}$ = 81 Hz, 3H, Pt(axial-CH_3)] (Figure S8). Partial ^{1}H NMR (400 MHz, 22 °C, acetone-d_6), δ: 1.40 (s, $^2J_{HPt}$ = 65 Hz, 3H, $PtCH_3$), 0.96 (s, $^2J_{HPt}$ = 80 Hz, 3H, $PtCH_3$). Only a partial ^{13}C NMR spectrum was acquired due to low solubility of **13**. ^{13}C NMR (150 MHz, 22 °C, HFIP), δ: 155.5, 146.1, 141.9, 137.9, 132.0, 127.5, 126.7, 126.3, 124.6, 122.7, 29.7 (2C overlapping, $^1J_{PtC}$ = 289 Hz). **13b**, ^{1}H NMR (400 MHz, 22 °C, acetone-d_6), δ: 8.69 (d, $^3J_{HH}$ = 5.7 Hz, 1H, pyridyl-*ortho* H), 1.25 (s, $^2J_{HPt}$ = 65 Hz, 3H, $PtCH_3$), 0.85 (s, $^2J_{HPt}$ = 69 Hz, 3H, $PtCH_3$). Other aromatic H and H from the CH_2CH_2 moiety produce signals overlapping with **13**. The **13**:**13b** ratio was 1:0.4 in MeCN-d_3

https://doi.org/10.1021/acs.organomet.2c00371
Organometallics 2022, 41, 2764−2783

(Figure S9) and 1:0.83 in acetone-d_6 (Figure S10). 1D selective ^{1}H NOE spectra: Figures S23 and 24.

4.9. Oxidation of 9 with H_2O_2 in Acetone, Isolation of 11c. Fifty milligrams (0.0834 mmol) of **9** was placed in a round-bottom flask with a stir bar. Eighty milliliters of acetone was added with stirring. Undissolved solid was filtered off if there was any. To the yellow/green solution was added 5 equiv (0.417 mmol) H_2O_2 (30% solution, aq, w/w). Then 0.5 h later, the solution became almost colorless and a large amount of white precipitate formed. The mixture was concentrated by a rotary evaporator, and then a centrifuge was used to separate the solid from liquid, which was discarded. Afterward, MeOH was mixed with the solid in the centrifuge tubes. Centrifugation was repeated, and liquid was discarded again. MeOH wash was repeated one more time before dissolving the white solid in HFIP. At last, HFIP was removed to give a white solid. The yield was 18 mg (37%). Crystals suitable for X-ray diffraction were obtained from super-saturated acetone or MeOH solutions. **11c**, ^{1}H NMR (400 MHz, 22 °C, DMSO-d_6), δ: 8.52 (d, $^3J_{HH}$ = 5.6 Hz, 1H, pyridyl-*ortho* H), 8.42 (d, $^3J_{HH}$ = 7.7 Hz, 2H, ArH), 8.30 (t, $^3J_{HH}$ = 7.9 Hz, 1H, ArH), 8.03−7.93 (m, 2H, ArH), 7.87 (d, $^3J_{HH}$ = 7.7 Hz, 1H, ArH), 7.51 (d, $^3J_{HH}$ = 7.8 Hz, 1H, ArH), 7.18−7.07 (m, 2H, ArH), 6.51 (t, $^3J_{HH}$ = 7.6 Hz, 1H, ArH), 5.25 (brs, 1H, OH), 3.65−3.52 (m, 2H, CH_2CH_2), 3.17−3.04 (m, 1H, CH_2CH_2), 3.02−2.89 (m, 1H, CH_2CH_2), 0.53 (s, $^2J_{HPt}$ = 64 Hz, 3H, $PtCH_3$). ^{1}H NMR (400 MHz, 22 °C, HFIP), δ: 8.90 (d, $^3J_{HH}$ = 5.4 Hz, 1H, pyridyl-*ortho* H), 8.25−8.17 (m, 2H, ArH), 8.02−7.93 (m, 2H, ArH), 7.86 (d, $^3J_{HH}$ = 7.7 Hz, 1H, ArH), 7.42 (d, $^3J_{HH}$ = 7.9 Hz, 1H, ArH), 7.33 (t, $^3J_{HH}$ = 7.6 Hz, 1H, ArH), 7.19 (dd, $^3J_{HH}$ = 7.9 Hz, $^3J_{HH}$ = 5.9 Hz, 1H, ArH), 6.82 (t, $^3J_{HH}$ = 7.6 Hz, 1H, ArH), 3.99−3.81 (m, 2H, CH_2CH_2), 3.39−3.26 (m, 1H, CH_2CH_2), 3.17−3.07 (m, 1H, CH_2CH_2), 0.86 (s, $^2J_{HPt}$ = 65 Hz, 3H, $PtCH_3$). The OH signal is hidden in the solvent signals (Figure S13). ^{13}C NMR (100 MHz, 22 °C, HFIP), δ: 167.0, 154.6, 152.5, 145.5, 144.8, 142.6, 141.2, 138.9, 137.1, 132.2, 131.4, 126.6, 126.3, 121.2, 82.3, 38.4, 28.3, −1.5. Two C signals are hidden in the solvent signals (Figure S14). ESI-MS: **11c** + K^+: 616.0257, calculated for **11c** + K^+: $[C_{20}H_{18}N_2O_4PtSK]^+$, 616.0267. 1D selective ^{1}H NOE spectra: Figure S19.

4.10. Isolation of 15 as a 1:2 Mixture with 11c. Fifty milligrams (0.0834 mmol) of **9** was placed in a round-bottom flask with a stir bar. Eighty milliliters of acetone was added to mix with the complex with stirring. The solid was filtered off if there was any. To the yellow/green solution was added 5 equiv (0.417 mmol) of H_2O_2 (30% solution, aq, w/w). Then 0.5 h later, the solution became almost colorless and white precipitate formed. The mixture was concentrated by a rotary evaporator, and then a centrifuge was used to separate solid from liquid. The acetone mother liquors were separated from solid complex **11c** and combined. After days to weeks, a white precipitate formed in the acetone mother liquor, which was collected by filtration. ^{1}H NMR was taken to show two species, **9** and **15**. Crystals of **15** suitable for X-ray diffraction were obtained from HFIP solution of the mixture above with a layer of Et_2O stored in a freezer in for 2 days. **15**, ^{1}H NMR (400 MHz, 22 °C, HFIP), δ: 8.51 (dd, $^3J_{HH}$ = 4.0 Hz,$^4J_{HH}$ = 0.7 Hz, 1H, pyridyl-*ortho* H), 8.24 (t, $^3J_{HH}$ = 8.2 Hz, 2H, ArH), 8.07 (d, $^3J_{HH}$ = 8.2 Hz, 2H, ArH), 8.03 (d, $^3J_{HH}$ = 7.7 Hz, 2H, ArH), 7.90 (d, $^3J_{HH}$ = 8.0 Hz, 2H, ArH), 7.81 (dd, $^3J_{HH}$ = 5.7 Hz, J_{HH} = 3.5 Hz, 2H, ArH), 7.60 (dd, $^3J_{HH}$ = 5.6 Hz, J_{HH} = 3.3 Hz, 2H, ArH), 7.51 (dd, $^3J_{HH}$ = 8.4 Hz, J_{HH} = 5.6 Hz, 2H, ArH), 7.42 (dd, $^3J_{HH}$ = 5.9 Hz, J_{HH} = 3.2 Hz, 4H, ArH), 3.76−3.55 (m, 4H, CH_2CH_2), 3.46−3.35 (m, 2H, CH_2CH_2), 3.20−3.11 (m, 2H, CH_2CH_2, overlapping with **11c**, 2.05 (s, $^2J_{HPt}$ = 58 Hz, 3H, $PtCH_3$) (see also Figure S16).

4.11. Oxidation of 8 with H_2O_2 in MeOH, Isolation of 10c. 11.5 mg (0.02 mmol) of **8** was mixed with 1 mL of MeOH (not fully soluble) under stirring. Five equivalents of H_2O_2 [0.010 mL, aq (aqueous), 30%, w/w] was added to the stirred mixture. Within seconds, the yellow suspension changed to a white one. Ten minutes later, filtration was performed to collect the white solid **10c**. The yield was 7.0 mg (63%). **10c**, ^{1}H NMR (400 MHz, 22 °C, DMSO-d_6), δ: 8.82 (d, $^3J_{HH}$ = 5.6 Hz, 1H, pyridyl-*ortho* H), 8.40 (dd, $^3J_{HH}$ = 8.6 Hz, *J*HH = 1.0 Hz, 1H, ArH), 8.29 (t, $^3J_{HH}$ = 7.9 Hz, 1H, ArH), 8.15−8.06 (m, 2H, ArH), 7.95 (d, $^3J_{HH}$ = 7.9 Hz, 1H, ArH), 7.89 (t, $^3J_{HH}$ = 7.9 Hz, 1H, ArH), 7.42 (t, $^3J_{HH}$ = 8.0 Hz, 1H, ArH), 7.19−7.09 (m, 2H, ArH), 6.72 (s, 1H, $CHSO_3$), 6.49 (t, $^3J_{HH}$ = 7.6 Hz, 1H, ArH), 5.40 (brs, 1H, OH), 0.53 (s, $^2J_{195PtH}$ = 67 Hz, 3H, $PtCH_3$) (Figure S11). Poor solubility of **10c** in commons solvents precluded acquisition of its ^{13}C NMR spectrum. Partial ^{1}H NMR (400 MHz, 22 °C, HFIP), δ: 1.73 (s, $^2J_{195PtH}$ = 76 Hz, 3H, $PtCH_3$). The **10b**:**10c** ratio was 1:2 in this solvent. ESI-MS of **10c** in HFIP solution: [**10c** + H]$^+$: 552.0515, calculated for $[C_{18}H_{17}N_2O_4PtS]^+$, 552.0558.

4.12. Isolation of 14. A HFIP solution of **10c** was layered with Et_2O and put in a fridge for 5 days. The crystals formed were collected, and a single crystal was characterized by X-ray diffraction.

4.13. Oxidation of 9 with O_2 in MeOH, Formation of 11d. *4.13.1. In MeOH-d_4.* Five milligrams (8.3 μmol) of **9** was mixed with 0.6 mL of MeOH-d_4 (not fully dissolved) in an NMR J Young tube in a glovebox. The NMR J Young tube was capped well and taken out of the glovebox to add 15 psi O_2 gas. The NMR J Young tube was left on a rotator and after 12 h, a small amount of crystalline solid precipitated. The crystals were determined by ^{1}H NMR to be **13**. ^{1}H NMR of the solution was checked without working up the mixture. Three major ligand-containing species showed up, namely, K[(L2)-Pt^{II}(OD)] (chemical shift of its terminal pyridyl *ortho*-H: 9.14), K[(L2)Pt^{II}(OCD_3)] (chemical shift of its terminal pyridyl *ortho*-H: 9.25), and **11d** (Figure S15). The NMR yield of **11d** (30%) was determined using 1,4-dioxane as an internal standard. Partial ^{1}H NMR spectrum of **11d** in the reaction mixture above (400 MHz, 22 °C), δ: 9.55 (m, 1H, terminal pyridyl *ortho*-H), 1.49 (s, $^2J_{HPt}$ = 71 Hz, 3H, $PtCH_3$). 1D selective ^{1}H NOE spectra: Figure S20.

4.13.2. In MeOH. In a similar reaction, a saturated solution of **9** in CH_3OH was used. The products NMR yields were determined using 1,4-dioxane as an internal standard: 12% for **13** and 31% for **11d**. The reaction mixture was analyzed by ESI mass spectroscopy with KPF_6 added. A strong signal at $m/z \approx 616$ was found with a proper isotopic distribution; the signal was assigned to **11d** + K^+. Partial ^{1}H NMR of **11d** in the reaction mixture above (400 MHz, 22 °C), δ: 9.55 (m, 1H, terminal pyridyl *ortho*- H), 1.48 (s, $^2J_{HPt}$ = 71 Hz, 3H, $PtCH_3$). ESI-MS(+), [**11d** + K]$^+$: 616.0160, calculated for $[C_{20}H_{18}N_2O_4PtSK]^+$, 616.0267.

K[(L2)Pt^{II}(OH)], partial ^{1}H NMR (400 MHz, MeOH-d_4), δ: 9.14 (m, 1H, terminal pyridyl *ortho*-H). K[(L2)Pt^{II}(OH)], ^{1}H NMR (400 MHz, D_2O), δ: 8.77 (m, 1H, terminal pyridyl *ortho*-H), 7.91 (m, 1H, L2), 7.66 (m, 1H, L2), 7.55 (m, 1H, L2), 7.53 (m, 1H, L2), 7.46 (m, 2H, L2), 7.36 (m, 1H, L2), 7.22 (m, 1H, L2), 7.09 (m, 1H, L2), 3.21−3.32 (m, 1H, L2), 3.10−3.16 (m, 1H, L2), 2.96−3.03 (m, 1H, L2), 2.59−2.67 (m, 1H, L2) (Figure S28). ESI-MS(−), [(L2)-Pt^{II}(OH)]$^-$: 562.0466, calculated for $[C_{19}H_{15}N_2O_4PtS]^-$, 562.0406.

K[(L2)Pt^{II}(OCH_3)], partial ^{1}H NMR (400 MHz, MeOH-d_4), δ: 9.25 (m, 1H, terminal pyridyl *ortho*-H). ESI-MS(−), [(L2)-Pt^{II}(OCH_3)]$^-$: 576.0470, calculated for $[C_{20}H_{17}N_2O_4PtS]^-$, 576.0562.

4.14. Oxidation of 9* in MeOH-d_4. Ten milligrams (88% purity, 11.8 μmol) of **9*** was dissolved in 0.6 mL of MeOH-d_4 in an NMR J Young tube in a glovebox. The NMR J Young tube was capped well and taken out of the glovebox to add 15 psi O_2 gas. ^{1}H NMR was taken intermittently. The reaction was finished in less than 5 h with a small amount of precipitate formed, which was determined to be **13**. Three major ligand-containing species showed up in solution, namely, ^{n}Pr_4N[(L2)Pt^{II}(OD)] (chemical shift of its *ortho*-pyridyl H: 9.14), ^{n}Pr_4N[(L2)Pt^{II}(OCD_3)] (chemical shift of its *ortho*-pyridyl H: 9.25), and **11d**. The products NMR yields were determined using 1,4-dioxane as an internal standard: 5% for **13** and 26% for **11d**. Partial ^{1}H NMR of **11d** in the reaction mixture above (400 MHz, 22 °C), δ: 9.55 (m, 1H, terminal pyridyl *ortho*-H), 1.48 (s, $^2J_{HPt}$ = 71 Hz, 3H, $PtCH_3$).

4.15. Oxidation of 9 with O_2 in MeOH, Formation of 11c. In a glovebox, 0.6 mL of a saturated solution of **9** in MeOH-d_4 was placed in a J Young NMR tube. The tube was removed from the glove box and pressurized with 15 psi O_2 gas. The NMR J Young tube was left on a rotator for 3 h, after which **9** was fully converted. Three

https://doi.org/10.1021/acs.organomet.2c00371
Organometallics 2022, 41, 2764−2783

major ligand-containing species showed up, namely, K[(L2)-$Pt^{II}(OD)$] (chemical shift of its *ortho*-pyridyl H: 9.14), K[(L2)-$Pt^{II}(OCD_3)$] (chemical shift of its *ortho*-pyridyl H: 9.25), and **11d** [chemical shift of its *ortho*-pyridyl H signal: 9.55, chemical shift of $PtCH_3$: 1.49 ($^2J_{HPt}$ = 71 Hz)]. The NMR J Young tube was then put in a 40 °C bath for 14 h, after which a white precipitate formed. The precipitate was collected and determined to be **11c** by ^{1}H NMR. Alternatively, **11c** could be obtained by allowing the solution after aerobic oxidation to stand for 2.2 days.

4.16. Oxidation of 9 with O_2 in 15 (vol) % TFE-Acetone, Formation of 23. 12.5 mg (0.0208 mmol) of **9** was mixed with 2.65 mL of acetone (not fully dissolved) in a 25 mL Schlenk tube containing a stir bar. Then, 0.468 mL (6.2 mmol) of TFE was added to the Schlenk tube to adjust the pH to ∼6.1. Next, 15 psi O_2 was pumped into the Schlenk tube before it was Teflon-sealed. It was then submitted to stirring for 12 h at r.t. After this time, all **9** was consumed. ^{1}H NMR of the reaction solution showed one major ligand-containing species assigned to a trifluoroethoxide anion adduct **23** (NMR yield: 61% using all signals in the aromatic region as a reference); **13** was produced in 17% NMR yield. Crystal growing was attempted after **13** was filtered off. The acetone solution was submitted to slow evaporation and solvent diffusion with Et_2O. Both attempts failed to produce crystals. Partial ^{1}H NMR of **23** in the reaction mixture above (400 MHz, 22 °C), δ: 9.18 (m, 1H, terminal py *ortho*-H), 1.28 (s, $^2J_{HPt}$ = 71 Hz, 3H, $PtCH_3$) (Figure S12). The reaction mixture (solid **13** removed) was analyzed by ESI mass spectroscopy with KPF_6 added. A strong signal at $m/z \approx 616$ was found with proper isotopic distribution; the signal was assigned to **11a** + K^+. ESI-MS(+), [**11a** + K]$^+$: 616.0244, calculated for $[C_{20}H_{18}N_2O_4PtSK]^+$, 616.0267. The reaction mixture was also analyzed by ESI mass spectroscopy in negative mode using aqueous MeOH as a mobile phase. The following well-resolved signals corresponding to **23** and derived species resulting from a facile anionic ligand exchange with the solvent were observed: ESI-MS(−): $[(L2)Pt^{IV}Me(OH)_2]^-$: 594.0453, calculated for $[C_{20}H_{19}N_2O_5PtS]^-$, 594.0668. $[(L2)Pt^{IV}Me(OH)(OCH_2CF_3)]^-$, **23**$^-$: 676.0, calculated for $[C_{22}H_{20}N_2O_5F_3PtS]^-$, 676.0698. $[(L2)Pt^{IV}Me(OMe)$-$(OCH_2CF_3)]^-$: 690.0918, calculated for $[C_{20}H_{19}N_2O_5PtS]^-$, 690.0855. 1D selective ^{1}H NOE spectra of **23**: Figure S21.

4.17. Oxidation of K[(L1)Pt^{II}Me], 8, with O_2 in MeOH, Formation of 12. K(L1)Pt^{II}Me, **8**, (10.8 mg, 0.02 mmol) was dissolved in MeOH (0.5 mL) in an NMR J. Young tube fitted with a Teflon valve under Ar. The solution was purged with O_2 for 1 min before the NMR tube was sealed. The reaction was monitored by ^{1}H NMR spectroscopy. A pale yellow precipitate formed after 4 h. The mixture was stirred (rotated) for an additional 2 h, and the precipitate was collected by filtration to give 5.3 mg of microcrystals (95% yield), which were identified by ^{1}H NMR as (L1)$Pt^{IV}Me_2$, **12**. No other species containing a $Pt^{IV}Me$ fragment were detected in the reaction solution. K[(L1)Pt^{II}(OH)], partial ^{1}H NMR (400 MHz, MeOH-d_4), δ: 9.14 (m, 1H, terminal pyridyl *ortho*-H), 5.94 (s, 1H, CH-bridge) (Figure S29).

K[(L1)Pt^{II}(OH)], ^{1}H NMR (400 MHz, D_2O), δ: 8.98 (m, 1H, terminal pyridyl *ortho*-H), 8.09 (m, 1H, L1), 7.77−7.82 (m, 2H, L1), 7.59−7.64 (m, 2H, L1), 7.43 (m, 1H, L1), 7.40 (m, 2H, L1), 7.30 (m, 1H, L1), 7.22 (m, 1H, L1), 7.10 (m, 1H, L1), 5.84 (s, 1H, CH-bridge) (Figure S27). ESI-MS(−), $[(L1)Pt^{II}(OH)]^-$: 536.028, calculated for [C17H13N2O4PtS]$^-$, 536.028.

K[(L1)$Pt^{II}(OCH_3)$], partial ^{1}H NMR (400 MHz, MeOH-d_4), δ: 9.29 (m, 1H, terminal pyridyl *ortho*-H), 5.91 (s, 1H, CH-bridge) (Figure S29). ESI-MS(−), $[(L1)Pt^{II}(OCH_3)]^-$: 550.0661, calculated for [C18H15N2O4PtS]$^-$, 550.0406.

4.18. Reductive Elimination of 11c. Here, 7.2 mg of **11c** was mixed with 0.55 mL of DMSO-d_6, 0.0552 mL (2.76 mmol) of D_2O, and 0.0266 mL (0.342 mmol) of CF_3COOD in an NMR J Young tube to get a suspension. Upon mixing, ^{1}H NMR was taken. A new single set of signals was observed, which was assigned to a protonated starting complex, **11c·H**$^+$. **11c·H**$^+$, ^{1}H NMR (400 MHz, 22 °C, DMSO-d_6), δ: 8.78 (d, $^3J_{HH}$ = 4.0 Hz, 1H, pyridyl-*ortho* H), 8.41−8.27 (m, 2H, ArH), 8.24 (d, $^3J_{HH}$ = 7.8 Hz, 1H, ArH), 7.99 (dd, $^3J_{HH}$ = 7.7 Hz, 1H, ArH), 7.95−7.85 (m, 2H, ArH), 7.55−7.48 (m, 1H, ArH), 7.47−7.40 (m, 2H, ArH), 3.50−3.02 (m, 4H, CH_2CH_2), 1.31 (br s, 3H, $PtCH_3$). The mixture was heated for 0.5 h at 80 °C. During this time, the suspension became a clear solution. Yields of products were determined by ^{1}H NMR integration using the total intensity of all aromatic H's as a reference and an additional prior calibration with respect to MeOH. CH_3OD (80%), CH_3OOCCF_3 (13%), and O=$S(CD_3)_2(CH_3)^+$ (4%) were detected. In terms of pincer ligand-containing species, two complexes were identified:

(L2)Pt^{II}(DMSO), **24**, (77%) and ($L2^{Me}$)Pt^{II}(DMSO), **25** (3%). (L2)Pt^{II}(DMSO), **24**, ^{1}H NMR (400 MHz, 22 °C, DMSO-d_6), δ: 8.81 (d, $^3J_{HH}$ = 5.5 Hz, 1H, pyridyl-*ortho* H), 8.21 (vd, $^3J_{HH}$ = 4.5 Hz, 2H, ArH), 8.12 (d, $^3J_{HH}$ = 7.7 Hz, 1H, ArH), 7.89−7.84 (m, 1H, ArH), 7.76 (t, $^3J_{HH}$ = 4.5 Hz, 1H, ArH), 7.72−7.69 (m, 1H, ArH), 7.62 (dd, $^3J_{HH}$ = 7.4 Hz, J_{HH} = 5.8 Hz, 1H, ArH), 7.30−7.22 (m, 2H, ArH), 3.15 (dd, $^3J_{HH}$ = 14.5 Hz, $^3J_{HH}$ = 9.6 Hz, 1H, CH_2CH_2), 2.84 (q, $^3J_{HH}$ = 10.5 Hz, 1H, CH_2CH_2). Two H from CH_2CH_2 are hidden under the water peak (Figure S17). (L2)Pt^{II}(DMSO), **24**, ^{13}C NMR (150 MHz, 22 °C, DMSO-d_6), δ: 164.7, 156.8, 156.0, 146.1, 142.3, 141.1, 140.9, 136.6, 134.0, 130.1, 125.4, 125.2, 124.7, 124.4, 119.1, 80.3, 36.1, 29.4 (Figure S18).

($L2^{Me}$)Pt^{II}(DMSO), **25**, partial ^{1}H NMR (400 MHz, 22 °C, DMSO-d_6), δ: 8.77 (dd, $^3J_{HH}$ = 5.4 Hz, J_{HH} = 0.9 Hz, 1H, pyridyl-*ortho* H), 8.19 (d, $^3J_{HH}$ = 5.9 Hz, 1H, py), 7.80 (d, $^3J_{HH}$ = 8.0 Hz, 1H, C_6H_3), 7.12 (vt, $^3J_{HH}$ = 7.6 Hz, 1H, C_6H_3), 7.08 (vd, $^3J_{HH}$ = 7.5 Hz, 1H, C_6H_3), 2.65 (s, 3H, CH_3Ph). Other H signals overlap with those of **24** and are not identified (Figures S25 and S26).

4.19. Reductive Elimination of a 2:1 Mixture of 11c and 15. Five milligrams of **11c** and **15** (molar ratio 2:1, pre-determined by ^{1}H NMR in HFIP) was mixed with 0.55 mL of DMSO-d_6, 0.0552 mL (2.76 mmol) of D_2O, and 0.0266 mL (0.342 mmol) of $DOOCCF_3$ in an NMR J Young tube to form a suspension. The NMR J Young tube was Teflon-sealed and heated for 0.5 h at 80 °C. During this time, the suspension became a clear solution. Yields of products were determined by ^{1}H NMR integration using the total intensity of all aromatic H's as a reference and an additional prior calibration with respect to MeOH. CH_3OD (88%; 3.17 ppm), CH_3OOCCF_3 (4%; 3.98 ppm), and O=$S(CD_3)_2(CH_3)^+$ (3%; 3.83 ppm) were detected. In terms of ligand-containing species, two complexes were identified, namely, (L2)Pt^{II}(DMSO), **24**, (53%) and ($L2^{Me}$)Pt^{II}(DMSO), **25** (5%).

4.20. Reductive Elimination of 11d. Five milligrams (8.3 μmol) of **9** was mixed with 0.6 mL of MeOH-d_4 (not fully dissolved) in an NMR J Young tube in a glovebox. The NMR J Young tube was Teflon-sealed and taken out of the glovebox to add 15 psi O_2 gas. The NMR J Young tube was left on a rotator for 12 h. ^{1}H NMR of the solution was checked to confirm the formation of **11d** and full conversion of **9**. Solid byproduct **13** was filtered off, and the reaction solution was transferred into a clean NMR J Young tube. An internal standard (20 μL of 0.200 M *tert*-butylbenzene in MeOH-*d*4) was added, and ^{1}H NMR was recorded. Then, 0.6 mL of D2O and 20 μL (0.26 mmol) of DOOCCF3 were added to the NMR J Young tube. The mixture was then submitted to heating at 80 °C for 0.5 h. A brown precipitate formed during heating. The ^{1}H NMR spectrum was checked after cooling the sample. Four pincer ligand-containing species were identified; no $PtCH_3$-containing species (no signals with Pt-195 satellites) were detected. Two new singlets emerged at 2.59 and 2.52 ppm that were assigned to CH_3 groups of C−C coupled products, ($L2^{Me}$)$Pt^{II}(OH_2)$, **30**, and $[(L2^{Me})Pt^{II}(O_2CCF_3)]^-$ or ($L2^{Me}$)Pt^{II}(MeOH). The combined yield of these two products based on the **11d** reacted was ∼100%. Addition of D_2O led to an increase in the intensity of the signal at 2.59 ppm (assigned to ($L2^{Me}$)$Pt^{II}(OH_2)$, **30**) at the expense of the intensity of the signal at 2.52 ppm assigned to ($L2^{Me}$)Pt^{II}(X). The third pincer ligand-containing species was identified as (L2)$Pt^{II}(OH_2)$, **29**, and the fourth one was proposed to be (L2)$Pt^{II}(O_2CCF_3)^-$ or (L2)-Pt^{II}(MeOH). (L2)$Pt^{II}(OH_2)$, **29**, partial ^{1}H NMR (400 MHz, 22 °C, MeOH-d_4), δ: 8.74 (d, $^3J_{HH}$ = 6.5 Hz, 1H, pyridyl-*ortho* H). ESI-MS of **29** in HFIP basified with KOH(aq): $[(L2)Pt^{II}(OH)]^-$: 562.0466, calculated for $[C_{19}H_{15}N_2O_4PtS]^-$, 562.0406. ($L2^{Me}$)-

https://doi.org/10.1021/acs.organomet.2c00371
Organometallics 2022, 41, 2764−2783

$Pt^{II}(OH_2)$, **30**, partial ^1H NMR (400 MHz, 22 °C, MeOH-d_4), δ: 8.74 (d, $^3J_{HH}$ = 6.5 Hz, 1H, pyridyl-*ortho* H). The solvent then was removed under vacuum, and the residue dissolved in DMSO-d_6. Two major pincer ligand-containing species were identified by ^1H NMR as (L2)Pt^{II}(DMSO), **24**, and ($L2^{Me}$)Pt^{II}(DMSO), **25** (Figure S25). A similar reaction with MeOH (6 mL), H_2O (5 mL), HBF_4 (92 μL, aq, 49%, w/w) instead of MeOH-d_4, D_2O, and $DOOCCF_3$ was carried out. The final reaction mixture was filtered, and then the solvent was changed from CH_3OH to TFE. This TFE solution was submitted to ESI mass spectroscopy with the eluent containing dilute HCl in aqueous AcOH. Anionic species were identified, with m/z values of 580.0062 (calcd. for $(L2)^{195}Pt^{II}(^{35}Cl)^-$, 580.0067) and 594.0343 (calcd. for $(L2^{Me})^{195}Pt^{II}(^{35}Cl)^-$, 594.0223).

4.21. Reductive Elimination of 11a (23). Five milligrams (8.3 μmol) of **9** was mixed with 0.53 mL of acetone-d_6 and 0.0936 mL of TFE (not fully dissolved) in an NMR J Young tube. The pH of the solution is calculated to be approximately 6.1. The NMR J Young tube was pressurized with 15 psi O_2 gas and Teflon-sealed. The tube with the mixture was left on a rotator for 12 h. The ^1H NMR spectrum of the solution was checked to confirm the formation of **23** and full conversion of **9**. Solid byproduct **13** was filtered off. The resulting solution was transferred into a clean NMR J Young tube, combined with an internal standard (10 μL of 0.196 M 1,4-dioxane in CD3CN), and a ^1H NMR spectrum was recorded. Then, 0.6 mL of D_2O and 20 μL (0.26 mmol) of CF_3COOD were added to the tube and mixed. The resulting clear light-yellow solution was then heated at 80 °C for 0.5 h. The ^1H NMR spectrum of the mixture was taken right after its cooling. Two pincer ligand-containing species were identified. No $PtCH_3$ signals were detected; a new singlet at 2.52 ppm emerged that was assigned to a C−C coupled product ($L2^{Me}$)-$Pt^{II}(OH_2)$, **30**. The NMR yield of **30** was 70%. By drying the liquid phase and dissolving the residue in DMSO-d_6, it was confirmed by ^1H NMR that one ligand-containing species is (L2)Pt^{II}(DMSO), **24**, and the other one is ($L2^{Me}$)Pt^{II}(DMSO), **25** (Figure S26).

4.22. Reductive Elimination of 10c. Complex **10c** is poorly soluble in pure DMSO even at elevated temperatures but dissolves in acidic DMSO solution (0.4 M CF_3COOD) after 2 h at 85 °C. After this time, a ^1H NMR spectrum of the mixture showed that **10c** underwent reductive elimination to produce MeOH (4% NMR yield) and MeO_2CCF_3 (87% yield), along with Me_3SO^+ (9%). Yields of the products were determined by ^1H NMR integration using the total intensity of all aromatic H's as a reference and an additional prior calibration with respect to MeOH. The pincer ligand-containing product was (L1)Pt^{II}(DMSO) reported earlier.[10] (L1)Pt^{II}(DMSO): ^1H NMR (400 MHz, 22 °C, DMSO-d_6), δ: 6.25 (s, 1H), 7.24−7.27 (m, 2H), 7.66−7.72 (m, 2H), 7.76 (dd, $^3J_{HH}$ = 6.0 Hz, $^4J_{HH}$ = 2.8 Hz, 1H), 7.88 (m, 1H), 8.00 (d, $^3J_{HH}$ = 7.6 Hz, 1H), 8.18−8.22 (m, 3H), 9.04 (d, $^3J_{HH}$ = 4.8 Hz, 1H). When **10c** was heated with 0.40 M CF_3CO_2H solution in D_2O at 85 °C for 2 h, the reaction resulted only in 1% yield of MeOH with the major product being a C−C coupled compound ($L1^{Me}$)$Pt^{II}(OH_2)$ exhibiting a singlet at 2.63 ppm.

4.23. DFT Calculations. Theoretical calculations in this work were carried out using a density functional theory method and a Jaguar program package.[35] Full geometry optimization was performed in the gas phase using the PBE functional and LACVP** relativistic basis set with polarization functions on all atoms except Pt. For all species under investigation, a frequency analysis was carried out. All energy minima were checked for the absence of imaginary frequencies, and all transition states possessed just one imaginary frequency. Using the method of intrinsic reaction coordinate, reactants, products, and the corresponding transition states were proven to be connected by a single minimal energy reaction path. The energies of the resulting stationary points were refined using single-point calculations at the PBE-D3/LACVP** level of theory in a necessary solvent (water, methanol, or acetone) utilizing the Poisson−Boltzmann continuum solvation model (PBF) as it is implemented in the Jaguar program package.[35]

■ ASSOCIATED CONTENT

Supporting Information

The Supporting Information is available free of charge at https://pubs.acs.org/doi/10.1021/acs.organomet.2c00371.

All experimental procedures, NMR spectra, and computational details (PDF)

Accession Codes

CCDC 2178554−2178560 contain the supplementary crystallographic data for this paper. These data can be obtained free of charge via www.ccdc.cam.ac.uk/data_request/cif, or by emailing data_request@ccdc.cam.ac.uk, or by contacting The Cambridge Crystallographic Data Centre, 12 Union Road, Cambridge CB2 1EZ, UK; fax: +44 1223 336033.

■ AUTHOR INFORMATION

Corresponding Author

Andrei N. Vedernikov − *Department of Chemistry and Biochemistry, University of Maryland, College Park, Maryland 20742, United States;* orcid.org/0000-0002-7371-793X; Email: avederni@umd.edu

Authors

Jiaheng Ruan − *Department of Chemistry and Biochemistry, University of Maryland, College Park, Maryland 20742, United States;* orcid.org/0000-0003-0907-5685

Daoyong Wang − *Department of Chemistry and Biochemistry, University of Maryland, College Park, Maryland 20742, United States*

Morgan J. Kramer − *Department of Chemistry and Biochemistry, University of Maryland, College Park, Maryland 20742, United States*

Peter Y. Zavalij − *Department of Chemistry and Biochemistry, University of Maryland, College Park, Maryland 20742, United States*

Complete contact information is available at: https://pubs.acs.org/10.1021/acs.organomet.2c00371

Notes

The authors declare no competing financial interest.

■ ACKNOWLEDGMENTS

This work was supported by the National Science Foundation (CHE-1800089) and, in part, by the Center for Catalytic Hydrocarbon Functionalization, an Energy Frontier Research Center funded by the U.S. Department of Energy, Office of Science, Office of Basic Energy Sciences, under award number DE-SC0001298.

■ REFERENCES

(1) Geletii, Y.; Shilov, A. Catalytic Oxidation of Alkanes by Molecular Oxygen. Oxidation of Methane in the Presence of Platinum Salts and Heteropoly Acids. *Kinet. Catal.* **1983**, *24*, 413−416.

(2) Lin, M.; Shen, C.; Garcia-Zayas, E. A.; Sen, A. Catalytic Shilov Chemistry: Platinum Chloride-Catalyzed Oxidation of Terminal Methyl Groups by Dioxygen. *J. Am. Chem. Soc.* **2001**, *123*, 1000−1001.

(3) Bar-Nahum, I.; Khenkin, A. M.; Neumann, R. Mild, Aqueous, Aerobic, Catalytic Oxidation of Methane to Methanol and Acetaldehyde Catalyzed by a Supported Bipyrimidinylplatinum−Polyoxometalate Hybrid Compound. *J. Am. Chem. Soc.* **2004**, *126*, 10236−10237.

(4) Hartwig, J. F. Evolution of C−H Bond Functionalization from Methane to Methodology. *J. Am. Chem. Soc.* **2016**, *138*, 2−24.

(5) Gunsalus, N. J.; Koppaka, A.; Park, S. H.; Bischof, S. M.; Hashiguchi, B. G.; Periana, R. A. Homogeneous Functionalization of Methane. *Chem. Rev.* **2017**, *117*, 8521−8573.
(6) Labinger, J. A. Platinum-Catalyzed C−H Functionalization. *Chem. Rev.* **2017**, *117*, 8483−8496.
(7) Vedernikov, A. N. Direct Functionalization of M-C (M = Pt^{II}, Pd^{II}) Bonds Using Environmentally Benign Oxidants, O_2 and H_2O_2. *Acc. Chem. Res.* **2012**, *45*, 803−813.
(8) Boisvert, L.; Goldberg, K. I. Reactions of Late Transition Metal Complexes with Molecular Oxygen. *Acc. Chem. Res.* **2012**, *45*, 899−910.
(9) (a) Stowers, K. J.; Kubota, A.; Sanford, M. S. Nitrate as a redox co-catalyst for the aerobic Pd-catalyzed oxidation of unactivated sp^3-C-H bonds. *Chem. Sci.* **2012**, *3*, 3192−3195. (b) Wang, D.; Weinstein, A. B.; White, P. B.; Stahl, S. S. Ligand-promoted palladium-catalyzed aerobic oxidation reactions. *Chem. Rev.* **2018**, *118*, 2636−2679. (c) Wang, Z.; Hu, L.; Chekshin, N.; Zhuang, Z.; Qian, S.; Qiao, J. X.; Yu, J.-Q. Ligand-controlled divergent dehydrogenative reactions of carboxylic acids via C−H activation. *Science* **2021**, *374*, 1281−1285.
(10) Watts, D.; Wang, D.; Adelberg, M.; Zavalij, P. Y.; Vedernikov, A. N. C−H and O_2 Activation at a Pt(II) Center Enabled by a Novel Sulfonated CNN Pincer Ligand. *Organometallics* **2017**, *36*, 207−219.
(11) Watts, D.; Zavalij, P. Y.; Vedernikov, A. N. Consecutive C−H and O_2 Activation at a Pt(II) Center To Produce Pt(IV) Aryls. *Organometallics* **2018**, *37*, 4177−4180.
(12) Munz, D.; Wang, D.; Moyer, M. M.; Webster-Gardiner, M.; Kunal, P.; Watts, D.; Trewyn, B. G.; Vedernikov, A. N.; Gunnoe, T. B. Aerobic Epoxidation of Olefin by Platinum Catalysts Supported on Mesoporous Silica Nanoparticles. *ACS Catal.* **2016**, *6*, 4584−4593.
(13) Vedernikov, A. N.; Shamov, G. A.; Solomonov, B. N. Theoretical Study of Oxidative Addition to Platinum Metal Complexes. VI. *fac*-Chelating Tridentate N- and P-donor Ligands as a Tool to Control Activity of Rh(I), Pd(II), Ir(I) and Pt(II) Complexes in Methane Oxidative Addition. *Russ. J. Gen. Chem.* **1999**, *69*, 1102−1114.
(14) Watts, D.; Wang, D.; Zavalij, P. Y.; Vedernikov, A. N. Novel Sulfonated CNN Pincer Ligands for Facile C−H Activation at a Pt(II) Center. *Israel J. Chem.* **2017**, *57*, 1010−1022.
(15) Kramer, M.; Watts, D.; Vedernikov, A. N. Catalytic Deuteration of $C(sp^2)$−H Bonds of Substituted (Hetero)Arenes in a Pt(II) CNN-Pincer Complex/2,2,2-Trifluoroethanol-d_1 System: Effect of Substituents on the Reaction Rate and Selectivity. *Organometallics* **2020**, *39*, 4102−4114.
(16) Khusnutdinova, J. R.; Zavalij, P. Y.; Vedernikov, A. N. Study of Aerobic Oxidation of Phenyl Pt^{II} Complexes (dpms)Pt^{II}Ph(L) (dpms = di(2-pyridyl)methanesulfonate; L = Water, Methanol, Aniline). *Can. J. Chem.* **2009**, *87*, 110−120.
(17) Ruan, J.; Wang, D.; Vedernikov, A. N. CH_3−X Reductive Elimination Reactivity of Pt^{IV}Me Complexes Supported by a Sulfonated CNN Pincer Ligand (X = OH, CF_3CO_2, $PhNMe_2^+$). *Organometallics* **2020**, *39*, 142−152.
(18) Vedernikov, A. N.; Binfield, S. A.; Zavalij, P. Y.; Khusnutdinova, J. R. Stoichiometric Aerobic Pt^{II}−Me Bond Cleavage in Aqueous Solutions to Produce Methanol and a Pt^{II}(OH) Complex. *J. Am. Chem. Soc.* **2006**, *128*, 82−83.
(19) Khusnutdinova, J. R.; Zavalij, P. Y.; Vedernikov, A. N. C−O Coupling of LPt^{IV}Me(OH)X Complexes in Water (X = ^{18}OH, OH, OMe; L = Di(2-Pyridyl)Methane Sulfonate). *Organometallics* **2007**, *26*, 3466−3483.
(20) Luinstra, G. A.; Labinger, J. A.; Bercaw, J. E. Mechanism and Stereochemistry for Nucleophilic Attack at Carbon of Platinum(IV) Alkyls: Model Reactions for Hydrocarbon Oxidation with Aqueous Platinum Chlorides. *J. Am. Chem. Soc.* **1993**, *115*, 3004−3005.
(21) Williams, B. S.; Holland, A. W.; Goldberg, K. I. Direct Observation of C−O Reductive Elimination from Pt(IV). *J. Am. Chem. Soc.* **1999**, *121*, 252−253.
(22) Williams, B. S.; Goldberg, K. I. Studies of Reductive Elimination Reactions To Form Carbon−Oxygen Bonds from Pt(IV) Complexes. *J. Am. Chem. Soc.* **2001**, *123*, 2576−2587.
(23) Pawlikowski, A. V.; Getty, A. D.; Goldberg, K. I. Alkyl Carbon−Nitrogen Reductive Elimination from Platinum(IV)−Sulfonamide Complexes. *J. Am. Chem. Soc.* **2007**, *129*, 10382−10393.
(24) Vedernikov, A. N.; Fettinger, J. C.; Mohr, F. Synthesis and Reactivity of Dimethyl Platinum(IV) Hydrides in Water. *J. Am. Chem. Soc.* **2004**, *126*, 11160−11161.
(25) Aseman, M. D.; Nabavizadeh, S. M.; Niroomand Hosseini, F.; Wu, G.; Abu-Omar, M. M. Carbon−Oxygen Bond Forming Reductive Elimination from Cycloplatinated(IV) Complexes. *Organometallics* **2018**, *37*, 87−98.
(26) Sberegaeva, A. V.; Liu, W.-G.; Nielsen, R. J.; Goddard, W. A.; Vedernikov, A. N. Mechanistic Study of the Oxidation of a Methyl Platinum(II) Complex with O_2 in Water: Pt^{II}Me-to-Pt^{IV}Me and Pt^{II}Me-to-$Pt^{IV}Me_2$ Reactivity. *J. Am. Chem. Soc.* **2014**, *136*, 4761−4768.
(27) Rostovtsev, V. V.; Henling, L. M.; Labinger, J. A.; Bercaw, J. E. Structural and Mechanistic Investigations of the Oxidation of Dimethylplatinum(II) Complexes by Dioxygen. *Inorg. Chem.* **2002**, *41*, 3608−3619.
(28) Abo-Amer, A.; Boyle, P. D.; Puddephatt, R. J. Push-Pull Ligands and the Oxidation of Monomethylplatinum(II) Complexes with Oxygen or Hydrogen Peroxide. *Inorg. Chim. Acta* **2020**, *507*, 119580.
(29) See Supporting Information for details.
(30) Clegg, D. E.; Hall, J. R.; Ham, N. S. NMR Studies of Aqua Exchange on Trimethylaquabipyridineplatinum(IV). *Aust. J. Chem.* **1970**, *23*, 1981−1987.
(31) Appleton, T. G.; Hall, J. R.; Ham, N. S.; Hess, F. W.; Williams, M. A. Kinetics of Site-Exchange Reactions in Di- and Tri-Methylplatinum(IV) Glycinate Complexes, from N.M.R. Lineshape Analysis. *Aust. J. Chem.* **1983**, *36*, 673−681.
(32) Hughes, R. P.; Meyer, M. A.; Tawa, M. D.; Ward, A. J.; Williamson, A.; Rheingold, A. L.; Zakharov, L. N. Does α-Fluorination Affect the Structural Trans-Influence and Kinetic Trans-Effect of an Alkyl Ligand? Molecular Structures of Pd(TMEDA)$(CH_3)(R_F)$ and a Kinetic Study of the *trans* to *cis* Isomerization of Pt(TMEDA)$(CH_3)_2I(R_F)$ [R_F = CF_2CF_3, $CFHCF_3$, CH_2CF_3]. *Inorg. Chem.* **2004**, *43*, 747−756.
(33) Liu, W.-G.; Sberegaeva, A. V.; Nielsen, R. J.; Goddard, W. A., III; Vedernikov, A. N. The Mechanism of O_2 Activation and Methanol Production by (di(2-pyridyl)methanesulfonate)Pt^{II}Me-$(OH_n)^{(2-n)-}$ Complex from Theory with Validation from Experiment. *J. Am. Chem. Soc.* **2014**, *136*, 2335−2341.
(34) Scott, J. D.; Puddephatt, R. J. Ligand dissociation as a preliminary step in methyl-for-halogen exchange reactions of platinum(II) complexes. *Organometallics* **1983**, *2*, 1643−1648.
(35) *Jaguar*, version 8.4; Schrödinger, LLC: New York, NY, 2014.

https://doi.org/10.1021/acs.organomet.2c00371
Organometallics 2022, 41, 2764−2783